ELSEVIER

Contents lists available at ScienceDirect

Ocean Engineering

journal homepage: www.elsevier.com/locate/oceaneng





SoJel –A 3D printed jellyfish-like robot using soft materials for underwater applications

Pawandeep Singh Matharu ^a, Zhong Wang ^d, John H. Costello ^b, Sean P. Colin ^c, Ray H. Baughman ^d, Yonas T. Tadesse ^a, *

- ^a Humanoid, Biorobotics and Smart Systems Laboratory (HBS Lab), Erik Jonsson School of Engineering and Computer Science, The University of Texas at Dallas, Richardson, TX, 75080, USA
- ^b Department of Biology, Providence College, Providence, RI, 02918, USA
- ^c Department of Marine Biology and Environmental Science, Roger Williams University, Bristol, RI, 02809, USA
- d Alan G. MacDiarmid NanoTech Institute, The University of Texas at Dallas, Richardson, TX, 75080, USA

ARTICLE INFO

Handling Editor: Prof. A.I. Incecik

ABSTRACT

Mass manufactured, biologically inspired soft robots are needed for safe robot-animal interactions. The key challenges are the design and manufacture of high-performance robots that meet stringent requirements in ocean environments. This work describes a 92% 3D-printed jellyfish-inspired soft robot, SoJel, which uses soft polymers for the bell and sensors. We show how slight variations in geometry affects the swimming performance of the robot, which demonstrates the need for advanced or custom-made 3D printers that avoid the difficulties in realizing controlled geometries by using traditional molding and casting techniques. The design reproduces important kinematic patterns of natural jellyfish, like the bell bending angle, actuation duty cycle, and bell kinematics. This work builds on previous generations of jellyfish-inspired robots that employed various types of actuators, but is largely polymer based, so it avoids metallic components that are susceptible to corrosion in the ocean. The realized cost of transport and vertical swimming height of robots powered by coiled nickel-titanium actuators are comparable to previous designs, however, the present robots have advantages in ease of design and manufacturing. A variety of soft robots and flexible structures can potentially be fabricated using this design principle. Flexible 3D-printed soft sensors enable us to determine the bending angles for motion estimation and control. Energy harvesting from water oscillation or free vibration is demonstrated using a twistron harvester and a piezoelectric composite integrated into the robot, which can be used for powering electronics, such as a LED for display and communication.

1. Introduction

Jellyfish (scientific name, Cnidarian medusae) are one group of underwater animals that have simple, unique, and efficient propulsion mechanisms. Jellyfish are known to have one of the highest energy efficiencies among all animal swimmers (Gemmell et al., 2013). They also possess a limited set of structural components compared to all other muscle-powered animal swimmers (J. H. Costello et al., 2008; J. H. Costello et al., 2021), making it easier to mimic for designers and prompting researchers to develop improved designs and potentially mass manufacture bioinspired underwater vehicles. Jellyfish swimming results from the contraction of the subumbrellar cavity, which produces a series of vortices by forcing fluid from the subumbrellar region (J.

Costello et al., 2019; Dabiri et al., 2006; Dabiri et al., 2005; Daniel, 1983). Study of hydrodynamic interactions during swimming by medusae–vortex formation and thrust production using particle image velocimetry (J. Costello et al., 2019) provides valuable information on the kinematics of real jellyfish for biomimetics. Efforts to replicate the propulsive motion of jellyfish for inspired vehicles have mainly focused on the method of actuation (Frame, Lopez, Curet and Engeberg, 2018b; Nawroth et al., 2012; Ren et al., 2019; Tadesse et al., 2012; A. Villanueva, S. Bresser, S. Chung, Y. Tadesse, & S. Priya, 2009a; A. Villanueva et al., 2011; N. W. Xu and Dabiri, 2020b; J. Yu et al., 2016). However, it became evident that more attention needs to be paid to the kinematics of bell motion that generates these hydrodynamic effects for successfully emulating them in jellyfish vehicles. Hence, based upon undisturbed

E-mail address: yonas.tadesse@utdallas.edu (Y.T. Tadesse).

^{*} Corresponding author.

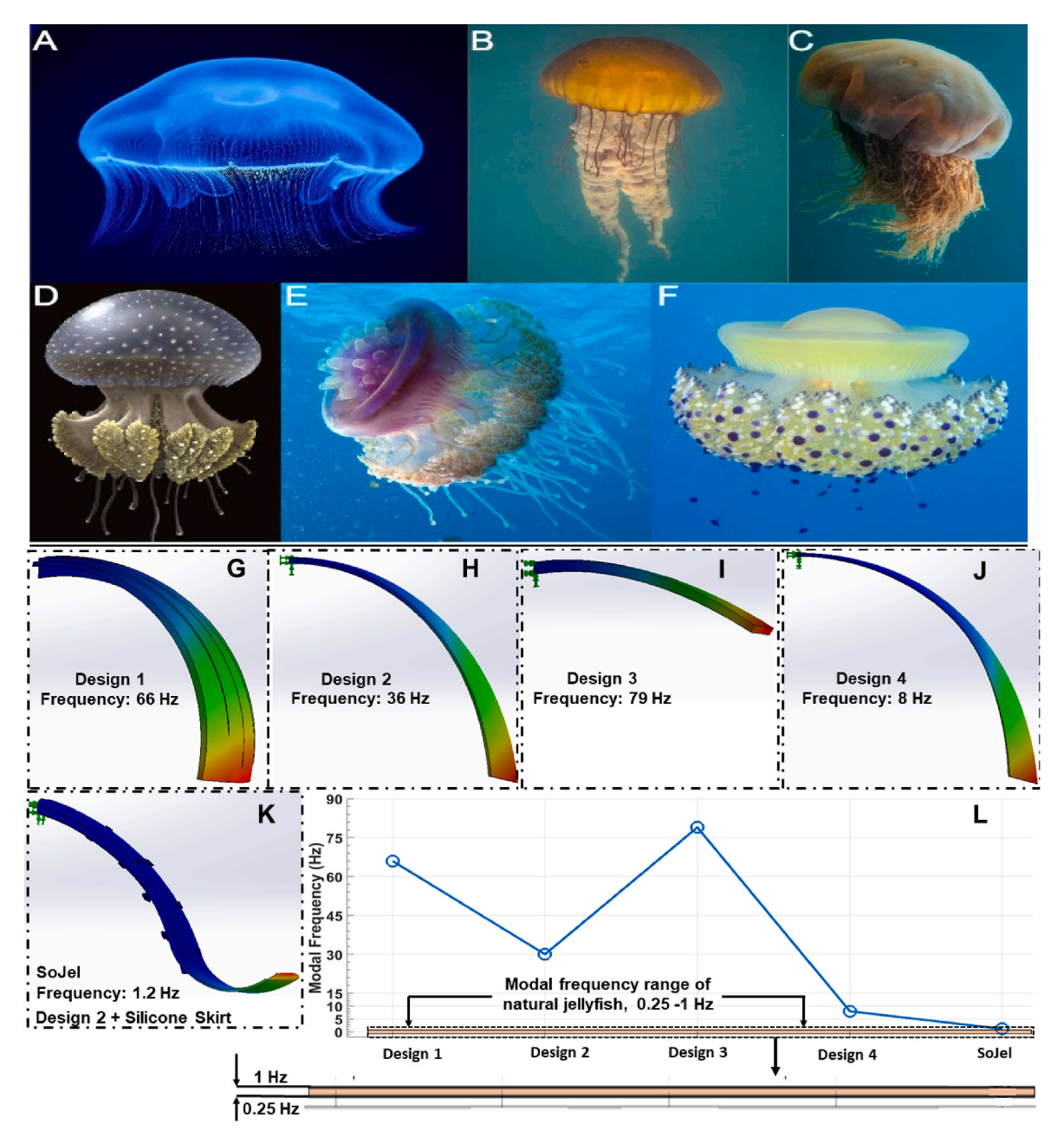


Fig. 1. Conceptual framework for determining the resonant frequency of 3D printed jellyfish bells. (A to F) Different species of jellyfish. Modal analysis results for (G) Design 1, (H) Design 2, (I) Design 3, (J) Design 4, (K) SoJel, (L) Comparison of Modal frequencies for Designs 1, 2, 3, 4 and SoJel (Design 2 with silicone bell).

swimming by animals in natural settings, we set general guidelines for biomimetic vehicles by considering three key parameters, *bell bending angle, duty cycle* and *bell curvature*. Our 3D printed robots were evaluated by considering these three key parameters, which were extensively characterized. There have been several biomimetic robots proposed for marine applications based on the common fish due to the unique advantage in underwater propulsion, control and maneuverability (Kadiyam and Mohan, 2019; Scaradozzi et al., 2017).

Despite clear evidence that resonance is widely exploited by animals, little work has focused on this aspect for biologically inspired underwater vehicles and robots. Investigations of fish swimming (Paraz et al., 2016) and insect flight (Ramananarivo et al., 2011) have used flexible materials for biological flapping foil propulsion. A variety of marine organisms, including squids, shellfish, octopuses, and jellyfish, utilize pulse-jetting by cyclic expansion and contraction for locomotion (Fig. 1A–F). Experiments and fluid dynamics modelling have led to the

development of a range of size-changing and pulse-jet robotic vehicles (Giorgio-Serchi et al., 2018; Krieg and Mohseni, 2008; Ruiz et al., 2011). Jellyfish robots have been developed that are driven by visible light (Yin et al., 2021a), dielectric elastomers (DE) (Cheng et al., 2018b; Christianson et al., 2019; S. Wang and Chen, 2021), ionic polymer metal composites (IPMC) actuators (Najem et al., 2012), piezoMEMS actuators (Alejandre et al., 2017), and untethered hydraulically-actuated silicone rubber tentacles (Frame et al., 2018b). Other pneumatically actuated jellyfish robots include the Fludojelly (Joshi et al., 2019), one of the fastest swimming jellyfish-inspired robots, swimming at speeds of 160 mm/s. However, none in literature have exploited either structural resonances or the 3D printability of soft materials. Bujard et al. (Bujard et al., 2021) identified the pulse-jet propulsion mode used in animals and demonstrated that resonance greatly benefits pulse-jet swimming speed and efficiency with a squid-inspired robot. Li et al. (T. Li et al., 2017) also presented a fast-moving soft-fish robot utilizing DE and an

ionic conductive hydrogel, but the required drive voltage was quite high. A soft actuator harnessing synergetic interactions between radio frequency—magnetic heating and coiled artificial muscles has been described, which can potentially be used in underwater soft robots in the future (M. Li et al.). Novel actuation methods have been recently presented, but these are millimeter-scale, for example soft millirobots for climbing three-dimensional surfaces (Wu et al., 2022). Other actuators like self-contained soft electrofluidic actuators (SEFAs) based on special dielectric liquid have been described for soft robot applications (Tang et al.). Zhang et al. (J. Zhang et al., 2022) developed hydraulically actuated bioinspired hydrogel jellyfish that has acoustic transparency, but they are molded.

The development of a mesoscale size soft jellyfish robot (300 mm-1 m in diameter) that can be 3D printed, thereby avoiding complex and time-consuming assembly, can create a paradigm shift in underwater closeup and minimally disruptive observations of marine life. One solution is to use compliant materials that enable the development of much safer (Y.-L. Park et al., 2014; Polygerinos et al., 2015), adaptable (Suzumori et al., 1992), and resilient (Tolley et al., 2014) biologically inspired robots (BIR) than its rigid counterparts. Octobot is one example in literature, which is entirely printed soft robot that is actuated by a fuel source (Wehner et al., 2016). However, its size is small (<100 mm) and upscaling the prototype for practical applications is difficult. Significant engineering challenges exist in the design, fabrication of scaled versions, and mass manufacturing of soft robots. Custom-designed molds have been the primary choice for fabricating soft robots that require multiple assembly steps (A. Hamidi, Y. Almubarak, Y. M. Rupawat, J. Warren, & Y. Tadesse, 2020b; Ilievski et al., 2011). These techniques are time-consuming, complex, and inconvenient when design changes are needed. We here mainly focus on the geometry, structural dynamics, and manufacturing associated with the swimming and actuation performance of the robot. Jellyfish robots like Kryptojelly (Almubarak, Punnoose, Maly, Hamidi and Tadesse, 2020b) and Poly-saora (Hamidi et al., 2020b), inspired by Tadesse et al. (2012), have shown vertical swimming actuated by shape memory alloy (SMA) wires and silver-coated nylon (TCPAg) artificial muscles, respectively. This approach can accommodate many actuation technologies (fuel-powered, electrothermal with coolant, electrochemical etc.). However, all these robots have rigid 3D printed structures with ABS plastic, and are assembled with molded silicone and spring steels, which are prone to corrosion and quickly damage. Another important aspect is that the SMA wires and TCP_{Ag} have small actuator strokes (<10%), which limit robot thrust. None of the studies in the literature have claimed the ability to entirely 3D print with soft material and the possibility for mass manufacture of a jellyfish soft robot.

To address the limitations of current prototypes, we conceived a scalable jellyfish-like robot design that can be 3D printed using soft materials and evaluated bell margin actuation and swimming. Wallin et al. (Wallin et al., 2018) examined the most relevant polymer systems for different elements of soft robots. They highlighted the advantages and limitations of different additive manufacturing processes for soft robotics. 3D printing of soft robots presents a promising approach to digitally design complex structures. Keneth et al. (Sachyani Keneth, Kamyshny, Totaro, Beccai and Magdassi, 2021) summarized the recent developments in the domain of materials for 3D printing of soft robots. Advancement in the field of soft grippers has been immense and Goh et al. (2022) has discussed about the use of 3D printing techniques for the fabrication of these soft robotic systems. This work also points to the potential of 3D printed soft sensors for smart grippers and paves a way for including them in other soft robotic applications.

A key challenge was to identify a 3D printable soft material, a geometry, and an actuation unit that has an operating frequency that falls close to the range of 0.1 Hz–1 Hz, like most natural jellyfish (Hoover and Miller, 2015; Miles and Battista, 2019; N. Xu et al., 2020; N. W. Xu and Dabiri, 2020a). This would allow the jellyfish robot to swim with a high amplitude of bell oscillation. However, we avoid operating right at the

resonance, as it is catastrophic and reduces the life cycle of the structure. Hence, understanding the impact of varying thickness of different bell designs was crucial for optimal actuation of the robotic bell and hence operation in marine environment for close monitoring of animals of other operations. In this study, we achieve the goal of actuating the robotic bell by using modal analysis for different designs (Fig. 1G–L), thereby obtaining a design having a modal frequency close to the swimming frequency range of jellyfish. NiTi actuator springs (Flexinol® spring) are used for obtaining large stroke actuation (\sim 200% stroke from loaded length when it is heated) and they have the ability to lift moderate loads that produce 172 MPa of stress.

The major contributions of this work in the design and development of swimming underwater robots that provide quiet operation (nonpneumatic, non-electromagnetic, and noise-free actuation) are:

- i) Based on observations of swimming jellyfish-like robots from the literature and the natural animal, we identified key patterns related to the hydrodynamic traits of the natural moon jellyfish (Aurelia aurita), such as asymmetric contraction, bell angle and duty cycle. These patterns are similar in other species, such as Black Sea nettle (Chrysaora achlyos), and we used them as guidelines for the design of the three prototypes that were evaluated experimentally. We followed the guidelines given in the results section, which can help in designing swimming bioinspired jellyfish robots in future for marine life exploration or other monitoring missions.
- ii) We identified the modal frequency of the bell and used the parameters for designing and demonstrating a swimming soft robot in which ~92% of the volume of the robot was fabricated by directly 3D printing soft materials. This is an important parameter in robot design, as it helps quantify the frequency range at which the bell actuation stroke is maximized. The key part of the robot was a thermoplastic polyurethane (TPU 92A) with a modulus 15.3 MPa, that is easily printed, and potentially more easily mass manufacturable with controlled geometry than would be robots made using a traditional molding process. 3D printing with TPU helps eliminate corrosion of metallic parts, as was seen in some jellyfish robots such as Robojelly (A. Villanueva et al., 2011), Kryptojelly (Almubarak, Punnoose, Maly, Hamidi and Tadesse, 2020a) and Poly-saora (A. Hamidi, Y. Almubarak, Y. Rupawat, J. Warren, & Y. Tadesse, 2020a). According to Regole, 2017, the material properties of TPU remain unchanged for a temperature range of -40 °C-125 °C (Regole, 2017) and the heat deflection temperature (HDT) of TPU is between 50 $^{\circ}$ C to 80 $^{\circ}$ C (Siemiński, 2021). The average surface temperature of the ocean varies from - 2 °C to 30 °C; depending on the regions, and temperature also varies based on the depth, the water is colder deeper in the ocean, but the average temperature is 4 °C (https://ocea nexplorer.noaa.gov/). Therefore, we can say that the TPU can sustain the temperature variation of the ocean environment. This approach and design consideration can be used manufacturing other underwater soft robots.
- iii) We demonstrated soft 3D printed piezoresistive sensors for bending angle estimation of the bell, which can be employed by other robots. We also demonstrated energy harvesting from ocean waves, by utilizing twisted and coiled carbon nanotube yarn energy harvesters (called twistron), and flexible piezoelectric composites to potentially provide supplemental power for future underwater robots.
- iv) We demonstrate the swimming performance of the jellyfish robot, compared with other molded and rigid robots in terms of vertical swimming height (h), cost of transport (COT) and size of the bell diameter (D). We found that 3D printability with soft material enables tailoring the geometry and associated performance of the bell more easily and more reliably for mass manufacture than would other methods.

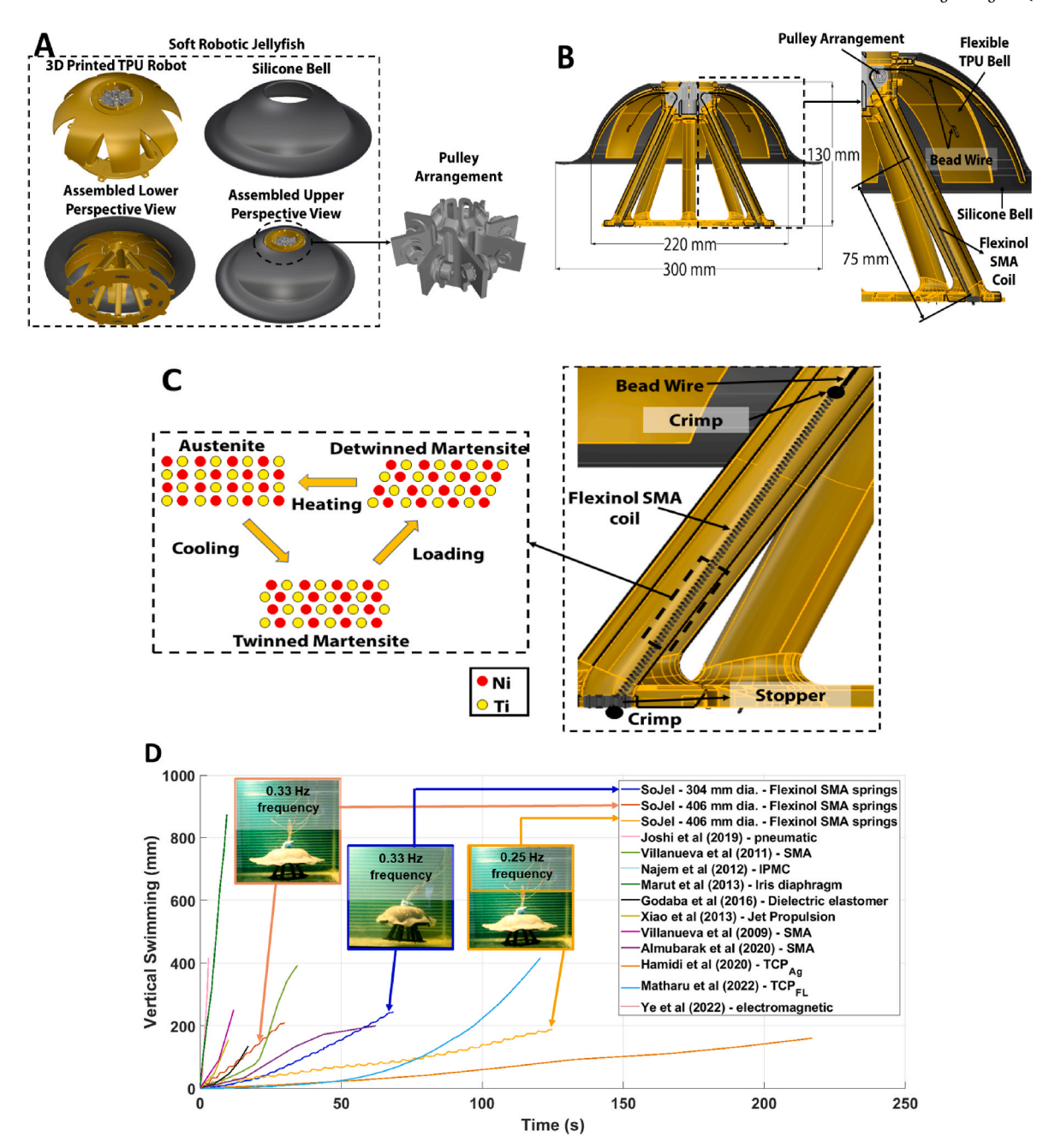


Fig. 2. 3D printed SoJel system overview. (A) CAD model and silicone bell skirt. (B) Sectional view of the robot with overall dimensions, detailed sectional view showing subcomponents. (C) Shape memory effect in NiTi SMA material, detailed view of actuator assembly inside passive cooling channels. (D) Comparison of vertical swimming displacement of different SoJels presented in this paper with other jellyfish-like biomimetic soft robots in the literature (Almubarak et al., 2020a; Godaba et al., 2016; Hamidi et al., 2020a; Joshi et al., 2019; Marut et al., 2013; Matharu et al., 2022; Najem et al., 2012; Alex Villanueva et al., 2009a; A. Villanueva et al., 2011; J. Xiao, J. Duan, & J. Yu, 2013; Ye et al., 2022). Some high performing miniature-sized (<15 mm) jellyfish robots (Ren et al., 2019; Ren et al., 2019; Yin et al., 2021b) are excluded from this swimming performance metric. Note: vertical movement vs time data of some jellyfish-like robots are not available or missing in publications (Frame, Lopez, Curet and Engeberg, 2018a; Tadesse et al., 2012), and therefore are not plotted here. Robots inspired from animals other than jellyfish are also excluded from this metric.

1.1. SoJel overview

We developed SoJel, a 3D printed biomimetic soft jellyfish robot with flexible TPU material that uses NiTi Flexinol® spring actuators as artificial muscles, which has an operating frequency within the range of actuation frequencies (0.25–1 Hz) of a natural jellyfish. It has flexible 3D printed sensors at the bell margin and an energy harvesting system that is integrated for harvesting wave motion as electricity. Though, this harvested electrical power is low compared with the required to actuate Flexinol® spring actuators, it can be used to power sensors and other

microelectronics for future applications, converting the free wave energy to electricity when the robot is at the base station and driven by ocean wave. The robot does not require assembly of different components, except the artificial muscles and pulleys. A 406-mm-diameter molded silicone skirt (for energy harvesting and sensor) is integrated on top of the 3D printed structure to mimic the motion behavior of a real jellyfish (Fig. 2A). For estimation of bending angle of the bell, we embedded 3D printed strain sensors that are flexible, piezoresistive, and quick in responding to changes in bending angles. We fabricated several sensors in our lab and evaluated the performance, which can be used for

Ocean Engineering 279 (2023) 114427

Table 1
Comparison of swimming jellyfish robots presented in the literature (Some high performing miniature-sized (<15 mm) jellyfish robots (Ren et al., 2019; Ren et al., 2019; Yin et al., 2021b) are excluded from this swimming performance metric).

Paper	Actuator	Voltage (V)	Current (A)	Power (W)	Frequency (Hz)	Weight (g)	Bell Diameter (mm)	Vertical Velocity (mm/s)
RoboJelly (A. Villanueva et al., 2011)	SMA wire	_	1.5	~100	0.5	242	164	50
JenniFish (Frame et al., 2018a)	PneuNet	-	-	2.29-5.85	0.8-0.435	380	210	30
DE Jellyfish (Godaba et al., 2016)	Dielectric Elastomer	6000	-	-	-	270	-	10
Modular Jellyfish (Zhou et al., 2016)	SMA wire	_	1	_	0.5	_	216	45
Untethered	Dielectric	7000-9000	_	_	1.6	28	156	5–10
Jellyfish (Cheng et al., 2018a)	Elastomer							
Synthetic Jellyfish (Kazemi-lari, Dostine, Zhang, Wineman and Shaw, 2019)	Coiled SMA spring	18–19	-	104–115	0.5	-	76	-
JetPRO (Marut et al., 2013)	Micro DC gear Motor	10	-	-	-	80	30	116
Fludojelly (Joshi et al., 2019)	Pneumatic (Air)	12	_	_	0.8	500	220	160
Kryptojelly (Almubarak et al., 2020b)	SMA wire	12	30	~360	0.33	650	210	60
Polysaora (Hamidi et al., 2020a)	6-ply TCP _{Ag}	20	60	~1200	0.25	440	210	5
LM-Jelly (Ye et al., 2022)	Electro-magnetic actuator	7.5	0.62	4.65	0.8	-	-	6
Jelly-Z (Matharu et al., 2022)	TCP_{FL}	60	1.8	~110	0.33	215	150	5.7
SoJel – 406 mm bell 0.33 Hz (This work)	Flexinol® SMA springs	10	60	600	0.33	~687	406	20
SoJel – 304 mm bell 0.33 Hz (This work)	Flexinol® SMA springs	10	60	600	0.33	~604	304	12
SoJel – 406 mm bell 0.25 Hz (This work)	Flexinol® SMA springs	10	60	600	0.25	~687	406	15

other applications as well. The overview of the robots can be found in movie \$1.

The pulleys and 3D printed ABS plastic components are the only rigid parts placed within an internal housing at the center of the bell (Fig. 2B). The stiffness of the TPU structure is sufficient to enable the bell to return to its non-actuated position, so there is no need to assemble the spring steels used in other state-of-the-art designs. A molded silicone skirt is employed to obtain high deformation that cannot be obtained using TPU materials. It also helped us in improving the swimming performance and the study on flexible bell margin effect. The silicone is Ecoflex 00–10 which is softer than TPU(Y.-L. Park et al., 2010; Smooth-On.com, 2022).

In this design, one Flexinol® spring actuator is integrated within each of the eight hollow channels for controlling each bell segment of the robot. Each of the actuators weigh 0.44 g, have a length of 17.5 mm and a wire diameter of 0.38 mm, a coiled wire diameter of 2.54 mm, a pitch of 1.1 mm per coil, and a resistance $R=3\,\Omega$, when the coils are under a load of 150 g. The working principle of a NiTi SMA is shown in (Fig. 2C). The arrangement is designed to enable convenient adjustment of pre-stress and easy replacement of artificial muscles (Fig. S1). When the silicone bell is included, the robot has a diameter of 406 mm and a height of 130 mm and weighs 687 g, which is 1560 times the weight of the SMA coils. It is made neutrally buoyant by adding a small piece of foam to the structure before each swim trial. Once the optimal design is 3D printed, the developed prototype is subjected to actuation tests underwater to match the angular displacement induced by the actuation of natural jellyfish (30–50°) (Colin et al., 2012; Nagata et al., 2016).

The Flexinol® spring actuators were characterized in water at 0.25 Hz under the needed load conditions to determine the optimal parameters for actuation of the SoJel. Thereafter, at least three successful vertical swim tests were conducted for each prototype in a 70-gallon capacity fish tank, which validates the concept of mainly 3D printing a soft jellyfish robot that provides characteristic swimming data for performance comparison. The swimming performance of the robot is comparable (Fig. 2D) to other jellyfish soft robots (Barbar et al., 2011; Hamidi et al., 2020a; Hareesh et al., 2016; Joshi et al., 2019; Marut et al., 2013; A. Villanueva, S. Bresser, S. Chung, Y. Tadesse, & S. J. Priya, 2009b; A. Villanueva et al., 2011; Jundong Xiao, Jinghui Duan, & Junzhi Yu, 2013). To limit the scope and focus on meso-to-meter scales, we have not compared jellyfish-inspired robots that are below 15 mm in diameter) (Nawroth et al., 2012; Ren et al., 2019; Ren et al., 2019; Yin

et al., 2021a) and other types of robotic robots like fish-inspired (Katzschmann et al., 2018), tuna-inspired, octopus-inspired robots, etc. Besides their swimming height, the comparison will be difficult to put in this short paper. For comprehensive comparison at all scales of state-of-the-art aquatic robots, great review papers on underwater robots are available (Bu et al., 2022; Y. Li et al., 2022; Raj and Thakur, 2016). We only compared jellyfish-inspired robots whose vertical swimming data is available. Table 1 compares important performance parameters of different SoJel prototypes with swimming jellyfish robots presented in the literature (Some high performing miniature-sized (<15 mm) jellyfish robots (Ren et al., 2019; Ren et al., 2019; Yin et al., 2021b) are excluded from this swimming performance metric). We also showed the energy harvesting capabilities of this robot in actual tested conditions by applying novel twistron energy harvesters (Kim et al., 2017; Lepró et al., 2012; Z. Wang et al., 2022; M. Zhang et al., 2005) and flexible piezoelectric composite, MFC strips. 3D printed strain sensors are shown that are piezoresistive and change resistance in response to applied bending or applied load.

1.2. Importance of this work

SoJel is the first largely 3D printed jellyfish-inspired biomimetic soft robot for potential applications in marine exploration. It is capable of swimming speeds comparable to that of more difficultly fabricated jellyfish robots found in literature (Fig. 2D). We can say that our approach follows the design for assembly (DFA) philosophy, as the number of components and the number of assembly operations to develop the robot is significantly reduced. This work demonstrates that 3D printed robots, with flexible TPU material having a silicone bell skirt, can achieve needed propulsive behaviors. This is in contrast to a 3D printed plastic robot that is much more rigid and has components which can corrode in underwater salty ocean environment (Almubarak et al., 2020a; Hamidi et al., 2020a) (Fig. S1 C). It also demonstrates the feasibility of using Flexinol® coiled NiTi spring actuators as a suitable material for vehicles of varying bell size, as well as energy harvesting for sustainability in an ocean environment.

Katzschmann et al. (2018) developed a fish robot named SoFi that is capable of close observations of marine life with its onboard sensors, control system and hydraulic actuation system. Robots like SILVER2 (Picardi et al., 2020), though bioinspired, use motors for exploring the

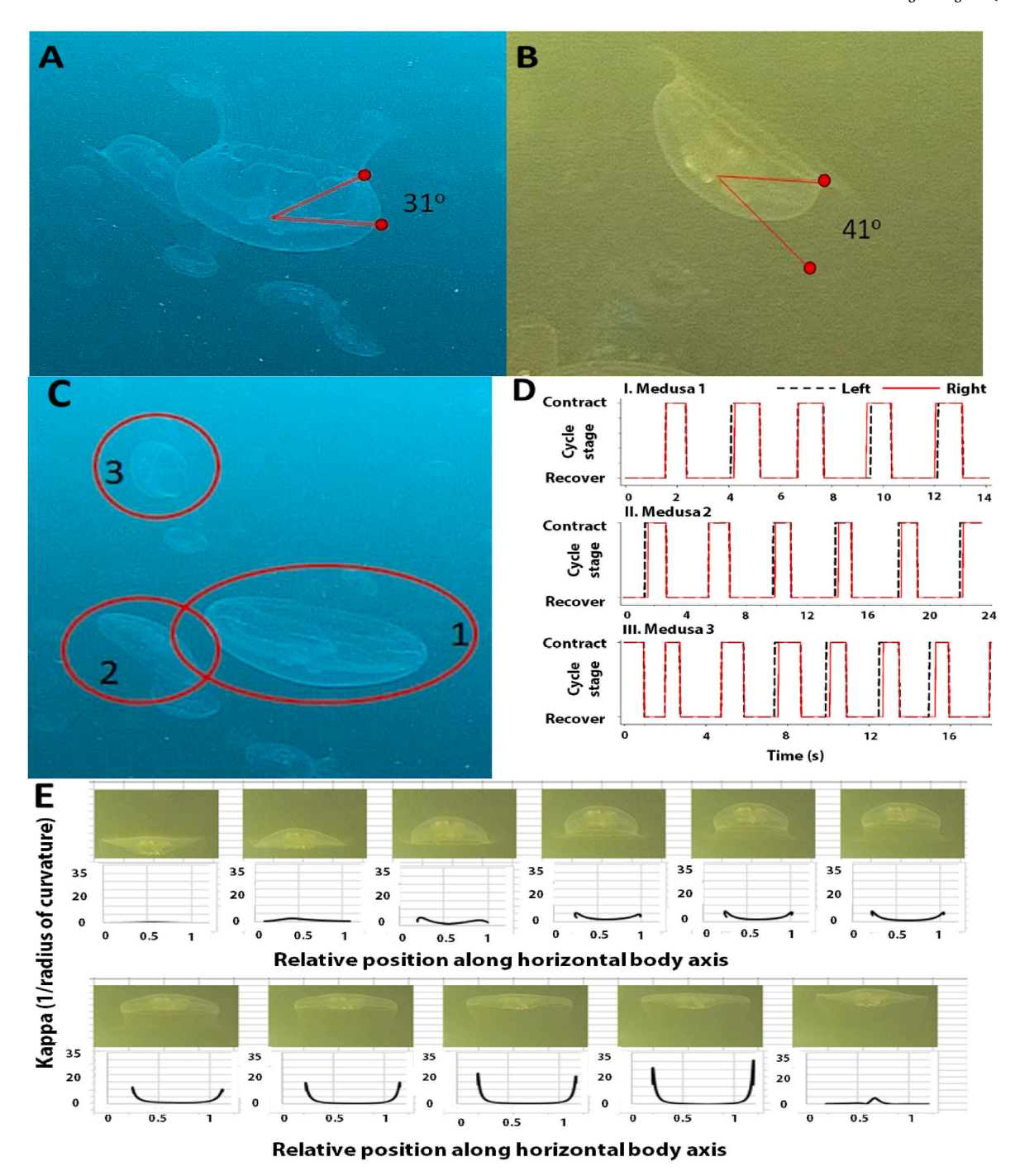


Fig. 3. Bell contraction by Aurelia aurita from different environments. (A) Mljet Lake, Croatia and **(B)** Greenwich Cove, RI, USA. Red circles represent the location of the bell margin at the initiation and termination of bell contraction during a pulsation cycle. **(C)** Coordination of bell margins (left and right) during pulsation cycles for in situ Aurelia aurita in Big Lake, Mljet, Croatia. **(D)** Timing of bell movement at the outset of contraction and recovery for three individuals swimming freely. Note that for any individual medusa, embedded within the rhythmic pattern of pulsation lies variability in the relative lengths of the contraction and recovery cycles. Additionally, the synchronization between contraction of margins on either side of the bell is highly variable. **(E)** Bell curvature during undisturbed in situ swimming by an *Aurelia aurita* medusa moving along a relatively linear vertical path (2° total direction change during complete pulsation). Note that the contraction phase (three left panels in first row) involves substantially less bending at the bell margins than the recovery phase (three right panels in second row). Hence, contraction and recovery are asymmetric motions.

seabed with legged motion. However, these works did not focus on fabrication, and they employed noisy electric motors for actuation. Our work provides an answer to the challenging problems of the prior work by using 3D printing soft materials for most of the robots and using noiseless artificial muscles as actuators.

Bujard et al. (2021) showed a squid-inspired robot using efficient resonant mechanism for the first time by using a coupled

mass-spring-mass oscillator. However, this work uses rigid mechanical and electrical components, which means that the robot is not soft, and it also involves assembly of many components. However, the SoJel is successful in achieving both softness and swimming. Mesobot (Yoerger et al., 2021), a 250-kg autonomous underwater robot addresses needs for observing and sampling in the ocean's midwaters. However, such rigid structured robots lack maneuverability, are hydrodynamically

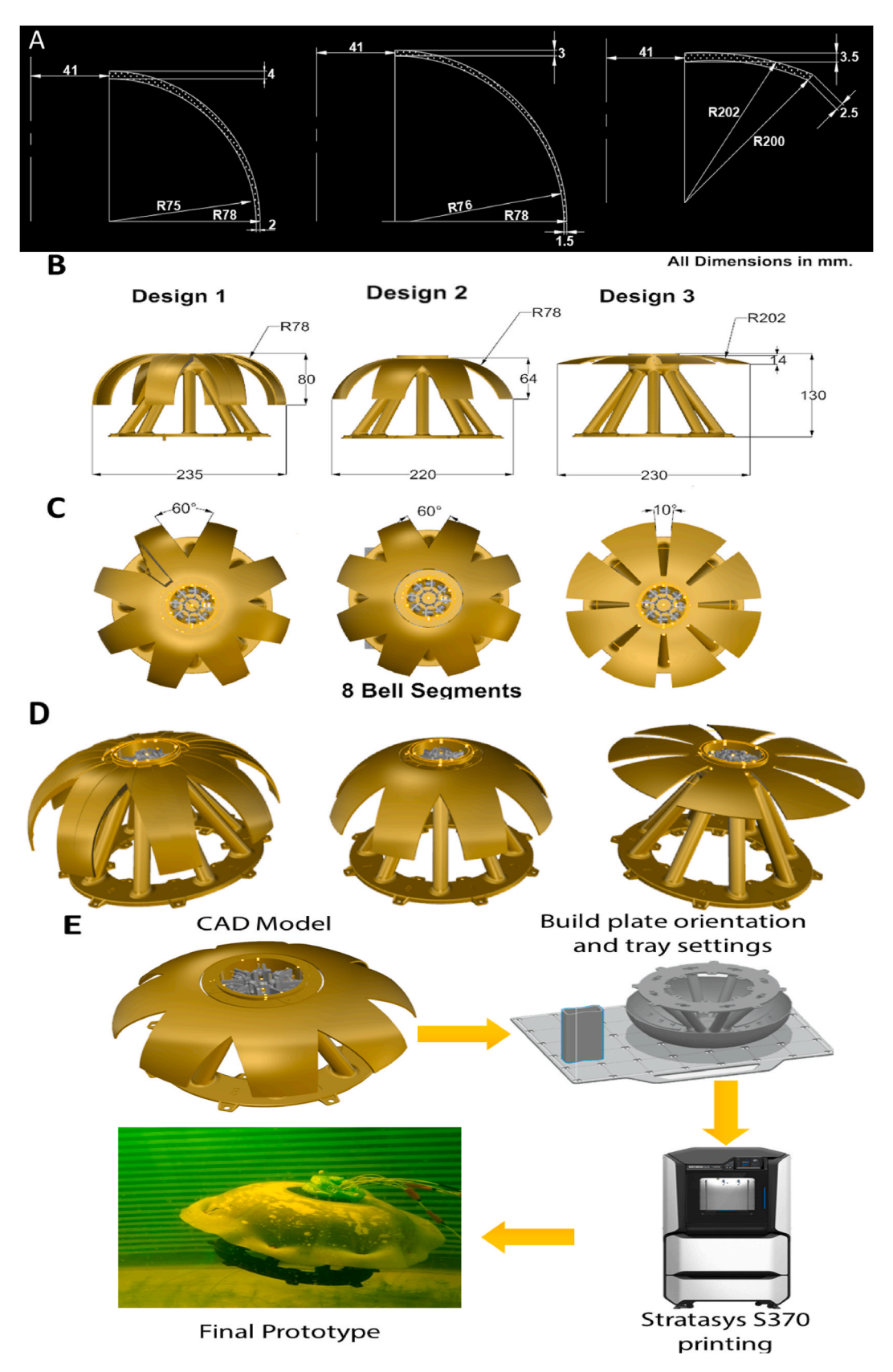


Fig. 4. Design of different prototypes of 3D printed soft jellyfish robot. (A) Schematic drawings for the three bell designs. These include different jellyfish bell dimensions. (B) Front views of the three 3D printable CAD models with relevant dimensions. (C) Top views of the designs. (D) Perspective views of the 3 designs. (E) Manufacturing process of a SoJel, including all steps to show the minimal assembly needed.

noisy, and less efficient swimmers compared to animal-inspired soft robots. In contrast to earlier robots, to simplify prototyping, SoJel is \sim 92% by volume 3D printed using a Stratasys F370 3D printer and a flexible thermoplastic polyurethane (TPU) (Table S2), obviating the need for complex molding techniques.

In this work, we first performed modal analysis based on guidelines for the design of bioinspired jellyfish robot and performed swimming experiments to determine the effect of bell margin on the TPU-based 3D printed robot. The bioinspired jellyfish design and fabrication, as well as associated performance related aspects, are examined by focusing on the cost of transport and swimming behavior. The next section will briefly describe the results.

2. Analysis, design, manufacturing methodologies

2.1. Structural dynamics - modal analysis of the bell

Identifying the dimensions and material properties is required to determine the desired structural resonance of a 3D printable bell, so that it is similar in behavior to a natural jellyfish. Having maximum actuation amplitude of the bell is critical for making a jellyfish-inspired robot efficiently swim. Therefore, a balance between actuation frequency and bending angle must be made. TPU material characteristics (Table S2) were used for four different designs, which were analyzed for a 1/8th segment of the bell of a jellyfish-inspired robot. The parameter variations for different designs were (i) the thickness of a uniform TPU cantilever beam, (ii) constant bell thickness vs variable bell thickness, and (iii) bell diameter (within the 3D printing limits of the printer, with 250 µm layer height) with the radius of curvature of different bells. In order to match the actuation frequency range (0.1-1 Hz) of natural jellyfish (Ahlborn et al., 2006; Demont and Gosline, 1988; Megill et al., 2005; N. W. Xu and Dabiri, 2020b) by using TPU, the bell thickness had to be small, as in design 4 (Fig. 1J). The thickness at bell center and at bell margin were originally set at 1 mm and at 0.5 mm, respectively. But, due to limitations of the 3D printer "Stratasys F370", this could not be fabricated, although this machine is one of the advanced commercially available 3D printers. Hence, design 2 (thickness at bell center of 3 mm, thickness at bell margin of 1.5 mm) was chosen. This design had a modal frequency of 30 Hz, which is higher than the frequency range of a natural jellyfish. Hence, a silicone bell skirt was molded and integrated with the TPU bell for design 2 (Fig. 1K), thereby reducing the modal frequency of actuation to 1.2 Hz. Consequently, design 2, integrated with molded silicone skirt on top, was chosen as the final prototype because this could be 3D printed and was closer to the actuation frequency range of a natural jellyfish. It is also closer to the actuation frequency of the Flexinol® spring actuators in water (0.25 Hz and 0.33 Hz) used in this paper. From this study, we concluded that in order to match the frequency of a natural jellyfish, the bell design must have a large bell diameter, a high radius of curvature, and a reduced thickness.

The model for finding the natural frequency of 1/8th portion of the bell segment is based on the Euler-Bernoulli beam equation when operating in air. The term for water inertia is not included as the modal analysis on SolidWorks was conducted without water as surrounding medium.

$$EI\frac{\partial^4 w(x,t)}{\partial x^4} = -\lambda_m \frac{\partial^2 w(x,t)}{\partial t^2} \tag{1}$$

where E is the modulus of elasticity, I is the moment of inertia, λ_m is the linear mass density of the beam (ρA , where ρ is the beams density and A is its cross-sectional area), w is the relative displacement, and t is the time. The resulting undamped natural frequency is given by

$$f = \frac{1}{2\pi} k^2 \sqrt{\frac{EI}{\lambda_m}} \tag{2}$$

Since this frequency depends on the modulus E and moment of

inertia, we explored various geometries by assuming the modulus of TPU to be constant.

2.2. Guidelines for bell margin actuation and kinematics for linear swimming

Before designing the robots, we reviewed successful swimming robots and natural jellyfish, wherein we observed three important parameters for design that we used as guidelines, as discussed at the beginning. The jellyfish animal model is selected due to energy efficiency and simple swimming mechanism, which has been discussed in many papers.

Bell bending angle: Considering animals in natural settings, we find that $30{\text -}50^\circ$ movement of the bell margin tips relative to the bell center is typical of contraction by natural organisms (Fig. 3 A, B). Margin actuation of this magnitude appears necessary to sufficiently propel an oblate jellyfish vehicle.

Duty cycle: The contraction duration should be substantially shorter than the recovery period. Although the ratios vary in nature (duty cycle = contraction/recovery of 0.4–0.6), contraction is generally half the duration of the recovery phase for Aurelia aurita in nature (Fig. 3 D).

Bending kinematics of bell margin (asymmetric contraction): The curvature of the bell, particularly the bell margin, increases during recovery compared to contraction during a pulsation cycle. The jellyfish bell is relatively flattened during contraction, except for some curvature near the margin. During recovery, the bell curves much more (>4 to 5X) as it unfolds to the relaxed, fully recovered position. This is highly pronounced at the bell margin. This pattern of straightened contraction, curved recovery is characteristic of many natural propulsors, including cilia (Biewener, 2003). Jellyfish bell margins demonstrate similar kinematic patterns to other biological propulsors - bending at the bell margin is more pronounced during bell recovery than during the contraction phase of the pulsation cycle. We have quantified curvature of bending using an index known as Kappa (K). Kappa is the inverse of the radius of curvature (ρ).

$$\rho = \frac{1}{\kappa} \tag{3}$$

The radius of curvature grows to infinity as a line straightens and kappa does the inverse and becomes infinitely small when a line is straight. Hence, low K means a straight section, high K means highly curved. The units are calibrated to the relaxed body diameter of the medusa at the outset of the turn, and it is assumed that magnification remains constant during the turn sequence. All units therefore are in body lengths. Total curve lengths never exceeded 1.2 of relaxed bell diameter. Bell contraction involves low K motions - relatively extended and straightened bell motions as the bell sweeps towards the center of the bell (Fig. 3 E). As bell contraction was completed, the bell margins curved inwards. Thus, the bell pulsation involves broad and extended bell configurations during contraction with curling the bell margin at the end of contraction. Bell recovery began with the contracted phase and magnified the pattern of increased margin curvature that began at the end of contraction. Bell recovery involved substantially greater bell curvature than does contraction. Hence, bell contraction and recovery involve fundamentally asymmetric motions.

2.3. Vehicle design and fabrication

The prototype discussed in this paper consists of a bell-like system with eight segments arranged symmetrically and driven into contraction-expansion angular displacement cycles by linearly actuating Flexinol® actuator springs through a pulley arrangement. The major dimensions of the first three designs are shown in Fig. 4A–D. Stratasys F370 with a nozzle diameter of 0.4 mm and build volume 355 \times 254 \times 355 mm was chosen for the fabrication of the robot, which determines the maximum overall dimensions of the soft robot. The layer thickness of

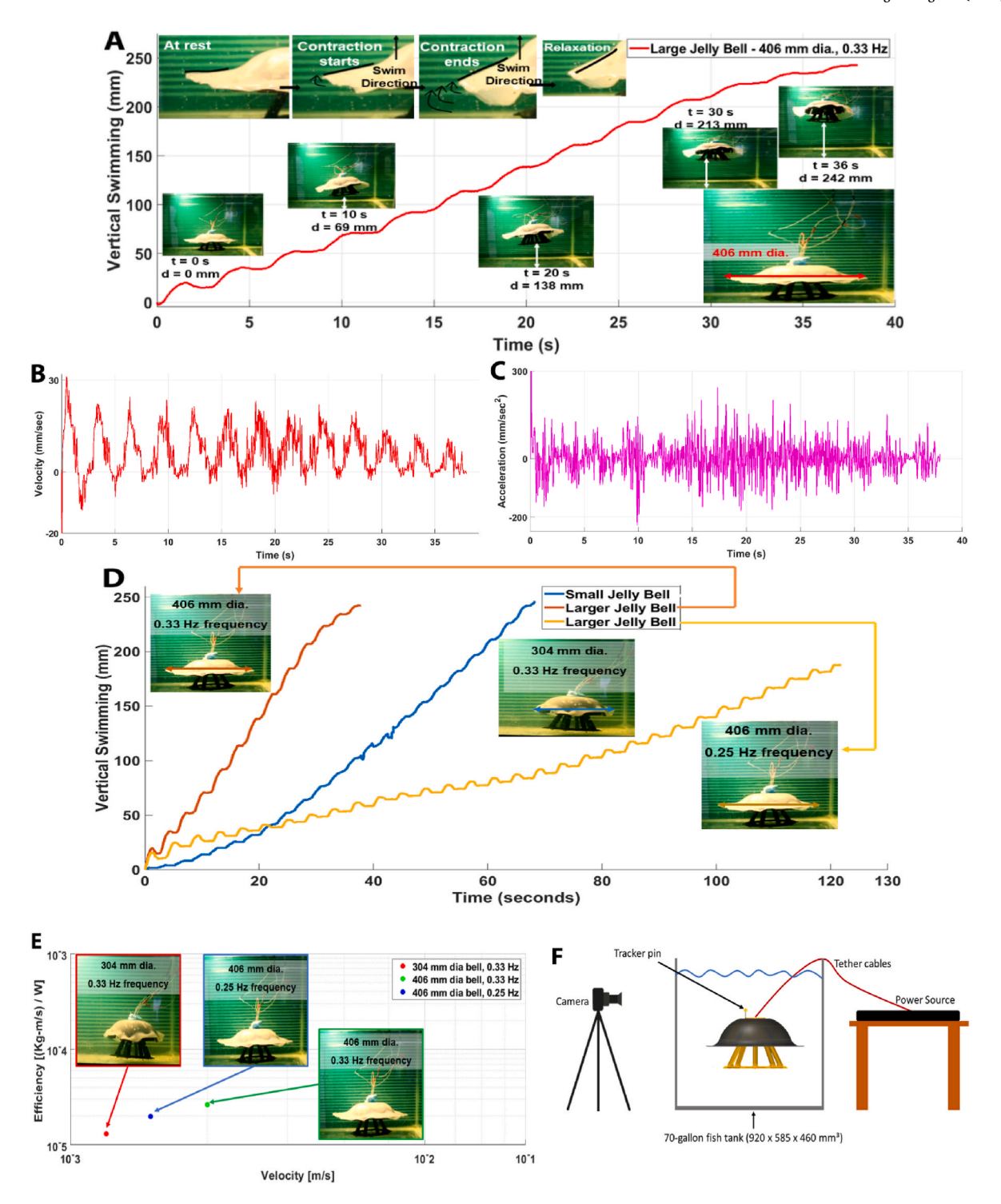


Fig. 5. (A) Biomimetic 3d printed jellyfish swimming test with SMA coils with 16-inch bell diameter showing vertical position at different time intervals and bell passive skirt deformation during actuation at 0.33 Hz/50% duty cycle, **(B)** Velocity vs time plot with quadratic fit, **(C)** Acceleration vs time plot with quadratic fit, **(D)** Comparison of swimming performance of SoJel with different bell margin sizes at different actuation frequencies, **(E)** Relationship between system velocity and locomotion efficiency defined as 1/COT (Ren et al., 2019) for SoJel for 304 mm dia. and 0.33 Hz actuation frequency, 406 mm dia. and 0.25 Hz actuation frequency, and 406 mm dia. and 0.33 Hz actuation frequency, (F) Free-swimming setup used for actuation tests in water.

print was 0.254 mm, infill 100%, printing speed was 20 mm/s while the material chosen to fabricate the robot was FDM TPU 92A (Stratasys, 2023). All the other process parameters for 3D printing are given in Supplementary Table S2. The print temperature was 230 $^{\circ}$ C, while bed temperature was kept at 50 $^{\circ}$ C. An upside-down orientation (Fig. 4E) was chosen for better print quality of the prototype.

The designs are made using CAD software keeping the following

parameters:

- i) The thickness of the bell suitable for TPU material printing
- ii) A constant bell thickness vs a variable bell thickness
- iii) The diameter of the bell within the 3D printing volume limit and resolution of the advanced commercial 3D printer

P. Singh Matharu et al. Ocean Engineering 279 (2023) 114427

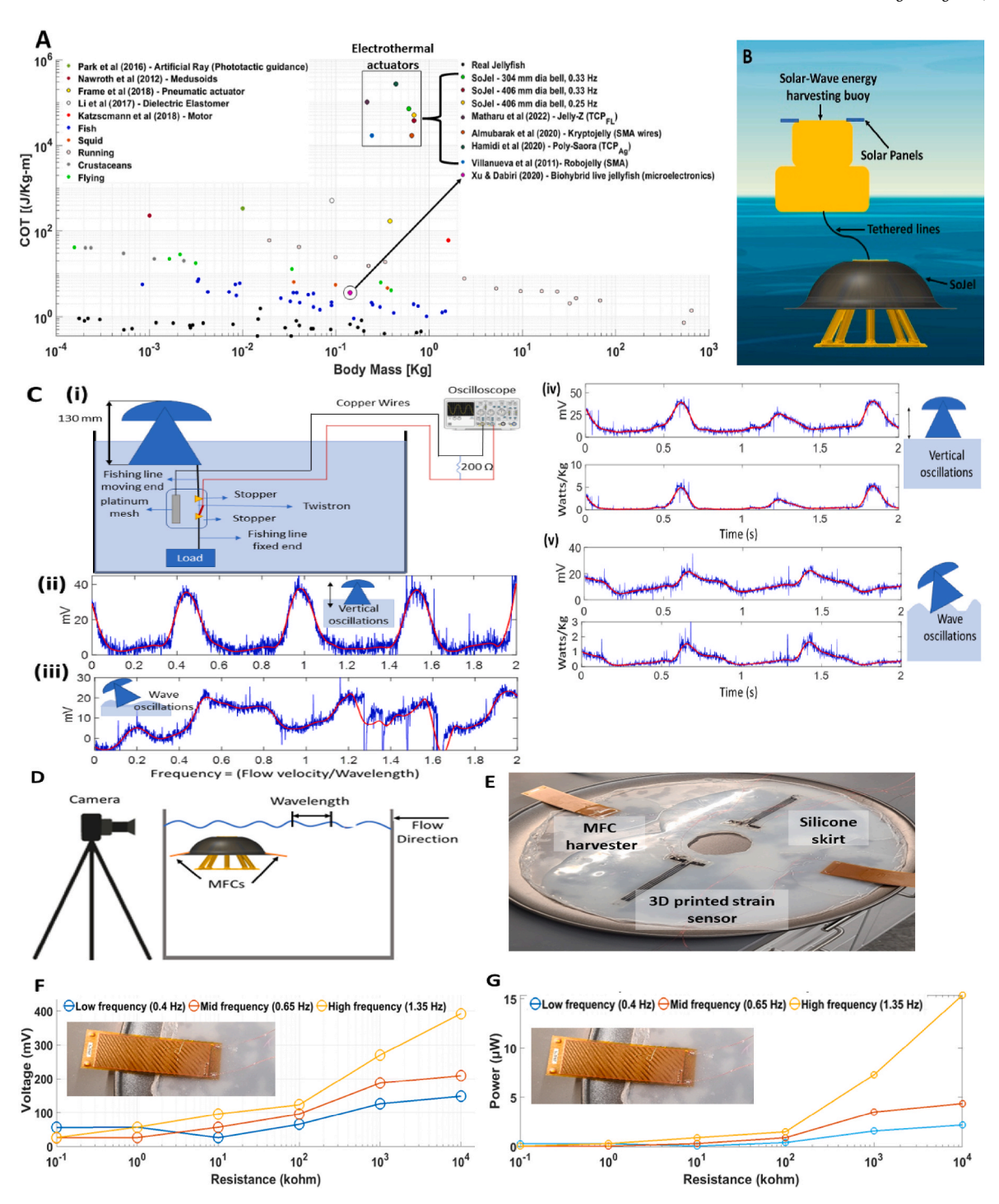


Fig. 6. Power aspects (A) Net cost of transport relative to body mass for SoJel prototypes, and for swimming, flying, and running animals (J. H. Costello et al., 2021), along with other major underwater robots bioinspired by different animals and also using different actuators (Almubarak et al., 2020a; Frame et al., 2018b; Hamidi et al., 2020a; Katzschmann et al., 2018; T. Li et al., 2017; Matharu et al., 2022; Nawroth et al., 2012; A. Villanueva et al., 2011; N. W. Xu and Dabiri, 2020b). For actual values, see Table S4. (B) SoJel concept with solar and wave energy harvesting, (C) Proof-of-concept of harvesting the ocean wave energy by twistron carbon nanotube yarn energy harvesters. (i) Schematics of the twistron harvester experimental set up. The time dependence of open circuit voltage for (ii) vertical oscillation and (iii) wave oscillation of the jellyfish. The time dependence of the generated voltage across a 200 Ohm resistor and the corresponding power output for (iv) vertical oscillation and (v) wave oscillation of the jellyfish, (D) Energy harvesting using MFCs when integrated in the jellyfish bell, (E) Arrangement of MFCs and 3D printed strain sensors on silicone skirt, (F) Voltage vs Resistance plot at different actuation frequencies for MFC 8528-P2 type, (G) Power vs Resistance plot at different actuation frequencies for energy harvesting.

2.4. Vertical swimming tests at different frequencies and bell skirt sizes

After the completion of design, 3D printing the soft structures, integration of 3D printed pulley system and characterization of one bell segment, discussed in Materials and Methods section, the SoJel was

tested for swimming with two different bell diameter skirt sizes (304 mm and 406 mm) and two different actuation frequencies (0.33 Hz and 0.25 Hz) for three different tests. The Flexinol® spring actuators would damage very quickly when actuated at 1.2 Hz (resonant frequency for SoJel). Therefore, 0.33 Hz and 0.25 Hz (actuation frequencies close to

Table 2Actuators investigated and potential actuators for future design of jellyfish inspired robots.

	•		<i>v v v</i>			
Actuation Technologies	TCP-6ply (Hamidi et al., 2020a)	TCP-fishing line with heater (Hamidi et al., 2019; Matharu et al., 2022)	Fishing Line hydrothermal mandrel coiled (Lianjun et al., 2015)	Sheath-run artificial muscle – Thermal (Mu et al., 2019)	Coiled SMA (Dynalloy, 2021)	Servo motors
Material	Silver-coated nylon 66	Nylon 66, fishing line with 0.08 mm nichrome	Nylon 66, fishing line	Carbon nanotube yarn with polyethylene oxide and a co polymer of tetrafluoroethylene- PFSA coated	Nickel and Titanium (NiTi)	Dynamixel servo Motors RX28
Actuation type Precursor fiber diameter (mm)	Electrothermal 0.2	Electrothermal 0.8	Hydrothermal 0.8	Electrothermal 0.05	Electrothermal 0.381	Electro-magnetic None
Precursor filament type	multifilament	monofilament	monofilament	monofilament	N/A	None
Diameter (mm)	2.4	2.8	3.3	0.1 [Mu et al., 2019]	0.10	Dimension: 35.5 mm × 50.8 mm x 41.8m
Resistance (Ω/mm)	0.031	2	-	-	0.00827	-
Force Lifting capability at max strain (g or MPa)	900 g	300 g	300 g	35 g	139 g	Holding Torque: 37kgf.cm (at 18.5V, 1.9A
Actuation stroke	17-20%	38%	30% at 90 °C water	13%	160% at 0.25 Hz	Unlimited
Contractile efficiency [%]	0.3	0.25	-	-	_	> 80%
Material cost [\$/kg]	2500	3070				
(Fishing line: 70, nichrome wire: 3000)	70	-	\$0.114/Coil	\$ 200 per item		
Contractile Power density (W/g)	In air: 4.3 In water: 0.3	-	-	9	-	37kgf.cm torque for 72 g m Mass actuator
Life cycle (cycles)	787 in water at 0.25Hz & 25% duty cycle	2400 in air at 0.009Hz & 1% duty cycle [Wu et al., 2018]			Million cycles in air	Can last for several years for intermittent operation

resonance frequency of this structure and within the frequency range of natural jellyfish) were chosen for swimming tests. As they are just below the resonant frequency of the SoJel bell, the amplitude of actuation would be close to maximum. SoJel (Design 2 with silicone skirt on top), swam vertically due to the contraction and relaxation of the bell segments that generate pressure gradient and vortex at the bell margin, which allowed the robot to propel upwards.

All Flexinol® spring actuators in the eight legs of the robot were connected in parallel, and a two-step power input (ON-OFF) was used for swimming tests. The robot was tethered to a DC power supply and a 60 A constant current, and a 10 V constant voltage was provided. This was based on good actuation (\sim 115% strain per Flexinol® SMA spring measured from its loaded length with 150 g m load) that was achieved in characterization tests done on a single bell. It must be noted that during all the swimming tests, SoJel was carrying a payload of \sim 687 g of its own structure, actuators, and tethered wires.

The first experiment was performed with a 16" (406 mm) diameter bell size of Ecoflex 00–10 silicone, using an actuation frequency of 0.33 Hz frequency and 50% duty. SoJel travelled a vertical distance of 250 mm in 35 s, the average velocity being 7.14 mm/s with instantaneous velocity of each cycle at 20 mm/s, and an instantaneous average acceleration at 100 mm/s^2 (Fig. 5A–C). The motion of the robot was more pronounced like a natural jellyfish than the smaller bell (304 mm diameter) (Fig. S2). It was observed that maintaining neutral buoyancy is very crucial for the robot. It can be seen from the plot in Fig. 5A that with each actuation cycle of 1.5 s, the robot pushes forward but falls due to its own weight for the relaxation interval (1.5 s). At this time, the actuators are cooled, and the bell returns to its original position.

The second and third swimming tests (explained in supplementary file, Fig. S2A and Fig. S3A) were conducted with 304 mm and 406 mm diameter bells, at 0.33 Hz and 0.25 Hz actuation frequency, respectively.

The third experiment was performed to relate the duty cycle of SoJel with the duty cycle of oblate jellyfish. The main objective here was to study the effects of bell margin design and actuation frequency on the swimming performance and to evaluate non-conventional actuators that actuate the bell to mimic the motion of a natural jellyfish. Fig. 5D compares swimming experiments conducted for the different abovedescribed bell diameters. It is noted that a larger passive skirt (20% of the bell, 78 mm on all sides) helps increase vertical displacement by decreasing asymmetries on bell sides during a pulsation cycle. Normal contraction of the silicone bell involves a large surface area in the direction of flow and the end of contraction cycle makes the bell margin bend inwards, like found in natural jellyfish. All three swimming experiments resulted in different average vertical swimming speeds (Fig. 5B, Fig. S4 B, Fig. S5 B). When the duty cycle was 50% (because 1.5 s heating and – 1.5 s cooling were used to obtain an actuation frequency of 0.33 Hz), the 406 mm bell diameter swims the fastest. It took 12 cycles and 35 s to reach the top of the experimental fish tank (250 mm of water column).

To describe the degree of success obtained from different swimming experiments, a comparison graph of locomotion efficiency against overall system velocity is plotted in Fig. 5E. A common metric for measuring propulsive efficiency, deployed by Ren et al. (Ren et al., 2019), is used for quantifying the effectiveness of biological locomotion techniques. It can be defined as the inverse of cost of transport (COT) (Paley and Wereley, 2020)

Efficiency
$$(\eta) = \frac{1}{COT} = \frac{mv}{P}$$
 (4)

where m, v, and P, are the mass (kg), velocity (m/sec) and power input (Watt) of the robot, respectively.

Fig. 5E shows that using a larger bell as a passive skirt increases the

Table 3Comparison of the kinematic patterns related to hydrodynamic traits of oblate jellyfish swimming to the experimental observations of the SoJel.

Characteristics	Oblate jellyfish swimming	3D printed jellyfish robot
Bell actuation Angle: bell margin tips relative to the centre of bell	30-50° is typical of natural organisms and successful vehicles.	\sim 10-12 $^{\circ}$ after the first actuation cycle (30-35 $^{\circ}$)
Duty cycle contraction/ recovery	Contraction duration is shorter than recovery period. Although the ratios vary in nature, the duty cycle is 0.4–0.6. Contraction is generally half the duration of the recovery phase for Aurelia aurita.	Duty cycle is 0.4–0.6 at an actuation frequency of 0.25 Hz. The 16-inch bell diameter integrated robot swims at a speed of ~1.5 mm/s (swims 180 mm in 120 s)
Bending kinematics	Curvature of the bell increases during recovery compared to contraction. The bell is relatively flattened during contraction, except for some curvature near the margin. During recovery, the bell curves much more (>4–5x) as it unfolds to the relaxed, fully recovered state.	The 16-inch diameter bell has a passive flap of more than ~2 inch on all sides, the bell is relatively flattened at the centre as the TPU printed soft robot is stiff near the centre, but there is curvature at the margin during the contraction phase. During recovery, the bell curves more and unfolds to the relaxed, fully recovered state.

efficiency of SoJel. The efficiency and speed of animals is generally higher than their robotic counterparts. Also, the cost of transport for different variants of SoJel are high when compared with jellyfish (Gemmell et al., 2013), fish, squid (J. H. Costello et al., 2021) etc., as seen in Fig. 6A. To somewhat decrease the COT, an active cooling mechanism, like shown by Lara-Quintanilla et al. (Lara-Quintanilla and Bersee, 2015), could be deployed. More importantly, electrochemically powered coiled carbon nanotube artificial muscles could be used, since they can be about as powerful as thermal muscles and can have contractile energy conversion efficiencies that are even higher than natural muscles. Xu and Dabiri (N. W. Xu and Dabiri, 2020b) have shown comparable COT with real animals but they have shown it in a biohybrid live jellyfish and not in a fabricated soft robot. Others shown in Fig. 6A (Frame et al., 2018b; Katzschmann et al., 2018; T. Li et al., 2017; Nawroth et al., 2012; S.-J. Park et al., 2016) have utilized pneumatic actuators, motors, dielectric elastomers, whose drawbacks, and unsuitability for making fully soft robots have already been discussed. We have explored several non-conventional actuators in the design phase of this robot. Table 2 compares possible actuators and some future actuators (electrochemical) that can reduce the power consumption. This shows that the work in this paper is a positive step towards manufacturing more energy efficient 3D-printed flexible soft robots with improved COT.

3. Discussion

We have presented extensive studies on design, development, and swimming performance of TPU printed biomimetic jellyfish soft robots, whose natural frequency of actuation is similar to the operating frequency of a natural jellyfish. These use a minimum number of components (less than 8% by volume) for ease of assembly. The robustness of the SoJel design helps in the fabrication of multiple vehicles that behave in the same way, for example as a colony of jellyfish. We focused on the controlled geometry of the robot, as the geometry and material of the bell segment are the key components for the swimming performance of the jellyfish inspired robot. The electrothermally driven Flexinol® SMA springs are great for design of underwater soft robots as they have very

high contraction percent and deliver repeatable, low-noise actuation. These materials can perform actuation at different frequencies within the actuation range of natural jellyfish. The only problem is that these actuators consume high power for actuation. Silicone casting has been one of the main manufacturing methods for fabricating soft robot prototypes, but this work aims to introduce the advancement of additive manufacturing and its potential application in soft robots. The purpose of 3D printing of the entire robot was to minimize the assembly and system integration (DFA principles). By doing so, we were able to eliminate the spring steel assembly that was used in prior state-of-art designs (Hamidi et al., 2020b; A. Villanueva et al., 2011). This resulted in corrosion free prototypes, since the entirely prototypes were made from up to \sim 92% by volume of flexible polymer parts.

We studied the bell margin actuation and kinematics for linear swimming of natural jellyfish as well as some previously developed prototypes and presented them as design guidelines for the development of jellyfish inspired soft robots. It is evident that the kinematics of bell motion that generate hydrodynamic effects is essential to successfully emulate them in the jellyfish vehicle. Table 3 provides a comparison summary of natural jellyfish and SoJel.

A silicone bell skirt was integrated with the robot, since it decreased the modal frequency. We can potentially replace the molded skirt with a 3D-printed very soft elastomer, which our group recently developed (Hamidi and Tadesse, 2019). All 3 swimming experiments presented were successful with different vertical swimming speeds. This work demonstrates the influence of different bell sizes, frequency of actuation, and duty cycle on swimming performance. Another important comparison criteria, the dependence of efficiency (1/COT) on velocity, shows that larger bell size produces higher velocity, while increase of actuation frequency will increase the overall efficiency of the robot as a system.

4. Limitations and future steps

For designing larger jellyfish robots, servo motors are efficient to deploy, due to very low power usage and sustainability in the ocean, but they are rigid and add to the weight of the robot. Artificial muscles should be used to change only a certain portion of the bell, perhaps along with a closed loop control system with servo motor actuation. Considering SMA actuators, research needs to be conducted in reducing the leakage of heat into the surroundings, which can increase the efficiency of these soft actuators, helping the robot to achieve efficiency closer to real animals. Hence, isolating the actuation unit from the surrounding should be done using an exhaust system.

To design a fully (100%) 3D printed robot, the actuators (NiTi) must be 3D printed (Elahinia et al., 2016) with the soft jellyfish robot, hence a design and manufacturing strategy has to be devised in future. We have recently achieved 3D printing of soft elastomer with silicone thinner agent that provides the highest elongation, reaching up to 1260% strain. This structure will be included in the future by using a bigger build plate. Our current custom-made silicone 3D printer has a build plate of 200 \times 200 mm which needs to be modified for a larger skirt size. Since dragonfly skin which is relatively softer than TPU, sustained high pressure at the deepest part of the ocean, TPU could withstand such high pressure at, if it is operated at deeper depths as shown by Li et al. (G. Li et al., 2021). It is preferable to have an actuation frequency of the bell structure that is close to resonance in order to take advantage of high deformation by tailoring the material properties and geometry. But we avoided operating right at resonance since the life cycle of the structure will be low in this region. As the Flexinol® springs are not able to operate optimally at 8 Hz frequency, a silicone bell was introduced having a lower natural frequency of 1.2 Hz, that is within the actuation frequency range of a real jellyfish. This made it easier for the artificial muscles to actuate the bell in a similar pattern to a real jellyfish. In the future to make it more suitable for practical applications such as inspection and manipulation (Pugi et al., 2018; Rumson, 2021; Sivčev et al., 2018), other systems must be integrated into the robot. A

Table 4Properties of Flexinol SMA springs under 2-step square-wave power input.

Material	90 °C Flexinol® (SMA) Actuator Spring			
Type of actuation	Electrothermal			
Wire diameter	$D = 0.381 \text{ mm}, D_O = 2.54 \text{ mm}$			
Solid Length	$L=17.5 \ mm$			
Mass (kg)	44×10^{-5}			
Resistance	$R=3\;\Omega$			
Input Current (A) (3-4 times higher than	6.5	7	7.5	
standard in air, 1.9 A)				
Output Voltage (V)	17.5	18.5	19.5	
Actuation power (W)	114	130	146	
Heating Time (s)	2			
Cooling Time (s)	2			
Duty cycle (%)	50			
Actuation frequency (Hz)	0.25			
Actuation Strain, at 150 g pre-stress	342%	400%	457%	
(experimentally found) ^a	(95%)	(100%)	(120%)	
Heating Pull Force standard (grams)	139			

^a The highest actuation strain is calculated from the unloaded length and the one in the bracket is the actuation strain from loaded length.

powering unit that can fit at the bottom of the robot is another work that we have been doing and this will be presented in the future. Such a powering unit will also address the issue of diving deeper, as currently the soft robot can dive to a depth allowed by the length of the tethering and will not impede its motion in any direction. Though the cables (flexible 24 AWG tinned copper hookup strand wires) powering the robot were used, the vertical swimming speed is affected a little bit. Hence, a separate powering unit needs to be fitted with the soft robot in future.

For this study, we selected coiled SMA actuators as they have consistent properties during actuation, are commercially available, and have higher strain under moderate stress than other actuators described in Table 2. We could have used twisted and coiled fishing line (TCP $_{FL}$) muscles with nichrome heating wire as shown by Matharu et al. (Matharu et al., 2022) or silver coated TCP as we showed in Hamidi et al. (2020b), but perfecting the manufacturing process is needed for large quantities. Artificial muscles, especially the thermally actuated ones are great for the design of underwater soft robots for quiet operation and stealth actuation. However, the power consumption of these muscles is very high, resulting in high COT values (Fig. 6A). Researchers have been struggling to solve this high-power consumption of SMAs for decades and have not yet solved it.

Power issues can be addressed by focusing on energy harvesting using solar power and actuating the robot while tethered to a surface water buoy (Fig. 6B) or harvesting ocean wave energy by integrating the twistron carbon nanotube yarn mechanical energy harvesters (Kim et al., 2017) (Fig. 6C). These twistrons have higher gravimetric output power densities than any other material-based technology. Twistron harvesters made of coiled carbon nanotube (CNT) yarns can convert mechanical energy to electricity in electrolytic medium (Kim et al., 2017). Because of the chemical potential difference between the CNT electrode and the surrounding electrolyte, these twistrons are automatically injected by a charge Q via electron or hole donation from the electrolyte. Stretching a coiled twistron yarn, having the same handedness of twist and coiling, increases yarn density and decreases yarn capacitance by C, while stretch release reverses this change. This stress-induced capacitance change produces a voltage change of V, according to the equation Q = CV, which enables the harvesting of mechanical energy as electrical energy (Fig. S11). Our recent study shows that the gravimetric peak output power for a 1 and a 30 Hz sinusoidal deformation are 0.73 and 3.19 kW/kg, respectively. This performance at 30 Hz is over 12-fold that of other prior-art material-based mechanical energy harvesters for frequencies between 0.1 and 600 Hz (Z. Wang et al., 2022). For a low wave motion, a twistron integrated in the jellyfish provides a power density of 6 W/kg. In addition, since the twistron

harvester can provide a quasi-linear change in the open circuit voltage with applied strain, they can be embedded into the bell of the jellyfish and used as a self-powered strain sensor for jellyfish movement control.

We also showed the use of energy harvesters for future applications of such underwater robots, where they can be utilized for powering sensors and other less power consuming electronic components in water. The powering issue can also be addressed by changing the actuation technology towards fuel-powered artificial muscles based on electrochemical muscles such as unipolar muscle (Chu et al., 2021) and sheath run muscles (Mu et al., 2019). Such muscles can be actuated using very low power, but the size of the jellyfish will be limited to $\sim\!100$ mm in diameter (Yang et al., 2020). However, for mesoscale robots and bigger size, such powering units should be further investigated for scalability. Nanomaterial coating of electrothermal actuators is a future research direction that can reduce the power consumption of these actuators with improved dynamic performance (Piao and Suk, 2020).

5. Materials, experiment and characterization

5.1. Experimental setup

The swimming performance results reported in Fig. 5D, were obtained from an experimental setup shown in Fig. 5 F. A standard video camera with a resolution of 720p (1280 x 720) was used to film the swimming experiments while a power source is kept beside the fish tank to power the robot for different parameters. The video analysis for measuring the vertical swimming displacement was conducted at a rate of 60 fps. A pin is attached at the top of the robot for tracking different positions at different time intervals. Video analysis was performed using open source "Tracker physics" software. A cardboard paper having stripes (8 mm wide) was attached in the swimming tank background and each stripe was taken as a measurement reference. Then the data was transferred to Microsoft Excel and plotted on MATLAB. The measurement accuracy depends on the water. For this reason, we often clean the water tank after performing experiments. The accuracy is also dependent on the step size and video frame rate. Therefore, we used 60 fps and a step size of 10 Hz to track the movement of the swimming robot.

5.2. Twistron energy harvester

As a proof-of-concept, twistron harvesters were connected to a robotic jellyfish and tested for harvesting wave energy and recording the voltage output in response to wave oscillation. Fig. 6C shows the schematic diagram of the set up. The twistron harvester was connected to the center of the jellyfish that floats on the water surface. The output power was measured by monitoring the voltage across a 200 Ω load resistor that was connected between twistron working electrode and a CNT wrapped Pt mesh counter electrode. Fig. 6C(ii), (iii) show the generated open circuit voltage with respect to the vertical oscillation and wave oscillation of the jellyfish. The open circuit voltage signal can be used for sensing the amplitude of the jellyfish oscillation. Using this set up, the generated power varies from 3 W/kg to 6 W/kg for different wave motion, which makes the jellyfish to be able to harvest energy from ocean surface (Fig. 6C (iv), (v)).

5.3. MFC energy harvesting

By embedding two 9528-P2 type MFCs diametrically opposite to each other in the silicone skirt (Fig. 6E), an experiment at different flow frequencies to show the feasibility of this concept was conducted at 1.35 Hz, 0.65 Hz and 0.4 Hz. The MFCs were connected to NI DAQ 9221 to measure the output voltage and determine the power obtained at different load resistances. It was found that with increase in resistance and flow frequency, the voltage and power outputs increased for the load resistance considered. The output voltage with different flow frequencies and load resistances varies from 40 mV to 400 mV while output

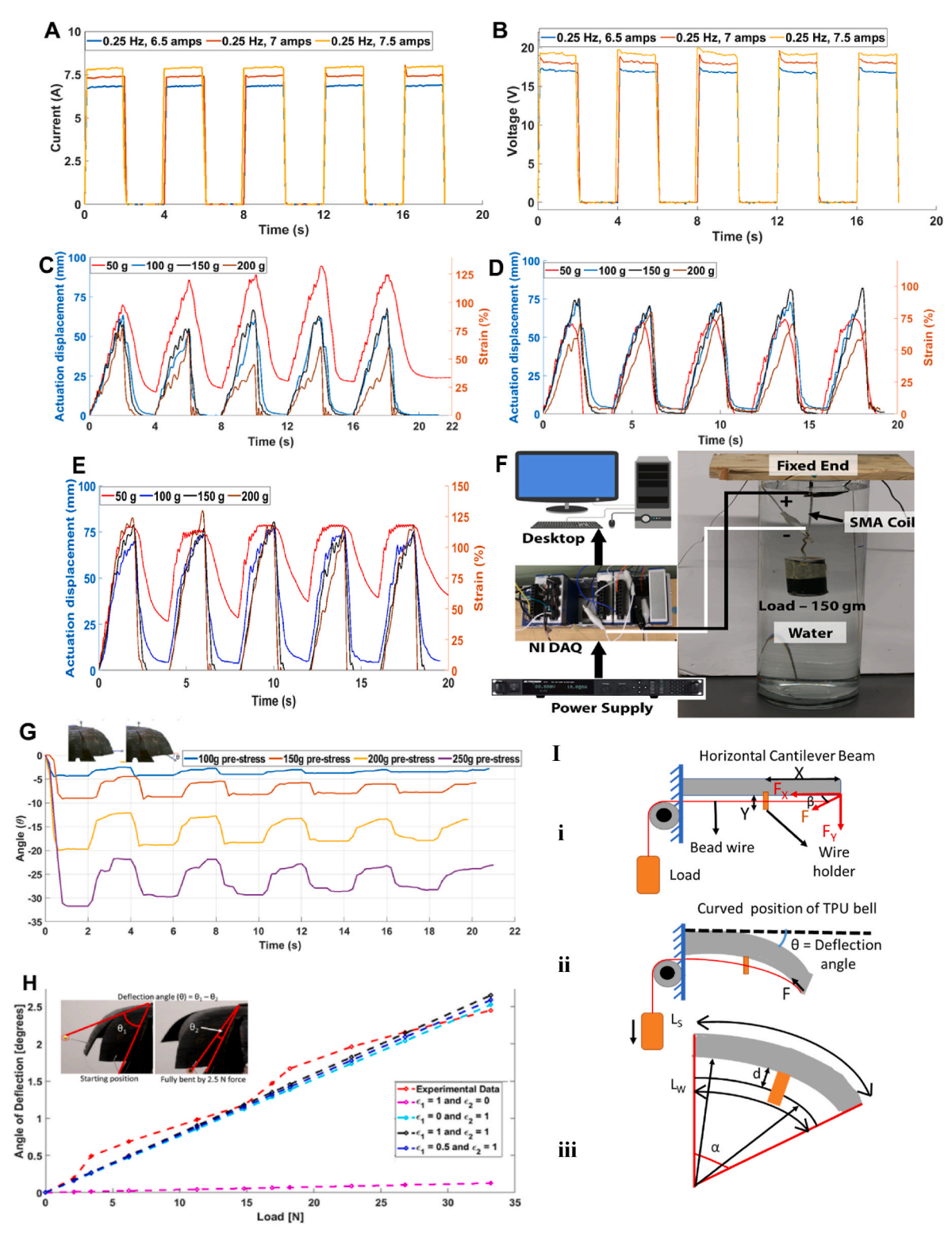


Fig. 7. Characterization of SMA coils and bell segment: (A)–(F) Characterization of SMA coils in water for five cycles at 0.25 Hz frequency and 50% duty cycle. Time dependence of (A) Current. (B) Voltage. (C) Actuator displacement (left) and actuator strain (right) of SMA coils at 6.5 A for different pre-stress loads. (D) Actuator displacement/strain at 7 A. (E) Actuator displacement/strain at 7.5 A. (F) Underwater Characterization setup for SMA coil actuators. (G)–(I) Static and dynamic deformation mechanism and analysis of the bell. (G) One bell segment actuation for the Design 2 prototype at 7.5 A input current for different pre-stress loads. (H) Vertical load compared with the theoretical results from the cantilever beam equation. (I) Bell deformation mechanism and curvature deformation angle (θ) for an applied load.

Table 5Material properties of conductive thermoplastic polyurethane (CTPU)(Ninjatek, 2023) for piezoresistive sensor.

Features & specifications	Values
Shore Hardness	90A
Tensile Strength (MPa)	12
Tensile Strength Elongation (%)	355
Tensile Stress at 50% Elongation (MPa)	8
Tensile Stress at 100% Elongation (MPa)	9
Tensile Stress at 300% Elongation (MPa)	11
Specific Gravity (g/cm ³) Print Guidelines	1.18
Extruder Temperature (°C)	220 to 230
Platform Temperature	 Room temperature to 45 °C
	 Glue is suggested on bed
Print Speed	 Top and bottom layers: 15–20 mm/s (900–1800 mm/min)
	• Infill speeds: 45–60 mm/s (2700–3600 mm/ min)
	 Layer 2+ use cooling fan if available.

power obtained varies from 0.1 μ W to 15 μ W. This shows the feasibility of this concept in future underwater robots to operate low-power electronics. The MFC can provide a voltage up to 40 V at higher vibration and frequency as can be seen in Uchino (2018), but our test was at low oscillation of water column in a lab setting.

5.4. Flexinol® actuator spring characterization

Characterization tests were conducted for understanding the material properties of the Flexinol® spring actuators which drive SoJel. Characterization on actuation time, pull force, cooling time, displacement and temperature have been carried out for this material (Daudpoto et al., 2012). There have been few studies that show the usage of SMAs in water that decreases the cooling time and aids in improving actuation frequency (Nizamani et al., 2017; Tadesse et al., 2010). Others have studied high actuation frequency of microscale SMA actuators up to 1 kHz (Lee et al., 2018) and the power density (Furst and Seelecke, 2012). The aim of this section is to study the parameters of the actuator useful for swimming. The experimental setup for underwater characterization of Flexinol® actuator springs (like the ones used for swimming experiments of SoJel), properties given in Table 4 is shown in Fig. 7 F. Four tests of varying pre-stress (50 g, 100 g, 150 g, 200 g) were conducted for three different input currents (6.5 A, 7 A, 7.5 A) at an actuation frequency of 0.25 Hz (50% duty cycle). Each cycle consisted of a heating step (2 s) and cooling step (2 s) while it continued for 5 cycles as shown in Fig. 7A-E.

The energy consumption for the actuator per cycle can be determined from the following equation,

$$E = Pt = VIt (5)$$

where P is power, and 't' is the time for which the power is supplied ($t=2\,s$). Using equation (5), the total energy consumption per cycle for 7.5 A input current is 150 J, which is quite high and can be a drawback, but there are possible solutions like using solar energy to power these robots (Fig. 6B) as shown in (Garcia-Cordova and González, 2013). The reason for such high input electrical power is that the actuator was tested in water, which helps to quickly cool the actuator. However, this water also drains out a lot of energy from the electrothermal actuator. A detailed study and more test results can be found in the supplementary file.

5.5. Bell segment characterization (experimental and theoretical study)

To study the swimming performance of SoJel, more attention is paid

to bell kinematics. Fig. 7G shows bell actuation using SMAs for prestresses of 100 g and 150 g. The first cycle actuates at an angular displacement of 38° , however for the following actuation cycles, the displacement is between 8° - 12° due to the response time of the SMAs.

To determine stiffness experimentally, weights ranging from 20 g to 250 g are used to bend the TPU bell. Fig. 7H shows the displacement of the TPU bell (2.5 mm average thickness and 80 mm length) under different static loads. Increasing the force, increases the bending angle as expected, but the key is the magnitude of angular stiffness 2.5 $\rm N/30^{\circ}$. Increasing the thickness, increases the stiffness of the bell, requiring a more powerful actuator that requires more energy to operate.

Theoretically, approximating the initial position of the TPU bell as a straight beam (Fig. 7I), the deflection is derived from superposition. This has been shown in Hamidi et al. (2020b) and we used Eq. (6) to evaluate the TPU bell.

$$\theta = \zeta_1 \frac{F_y L^2}{2EI} + \zeta_2 \frac{ML}{EI} = \zeta_1 \frac{F_y L^2}{2EI} + \zeta_2 \frac{F_x L d}{EI}$$
 (6)

where θ is the deflection angle, F_x is the force acting parallel to beam, F_y is the applied perpendicular force, d is the shortest distance between the bell and the wire, E is the modulus of elasticity of TPU 92 A (15.3 MPa), I is the moment of inertia, E is the bell segment length, and E is the bending moment due to E is the bell segment factors, which have been introduced for simplicity and used to correct for the small angle approximation.

Analytical results using Eq. (6) and the experimental results are shown in Fig. 7H. When $\zeta_1=1$ and $\zeta_2=0$, the deflection is due to the y-direction force, whereas, when $\zeta_1=0$ and $\zeta_2=1$, the deflection occurs due to the horizontal force. The best approximation of the experimental results came when $\zeta_1=0.5$ and $\zeta_2=1$, and $\zeta_1=1$ and $\zeta_2=1$. Eq. (6) is generally used for small deflection analysis; however, it is interesting to note that with the correction factors (ζ_1 and ζ_2), the tip deflection is correlated with the small angle assumption.

5.6. 3D printed flexible strain sensors

To study bell deformation and realize the entire system using additive manufacturing, we 3D printed flexible strain sensors using inexpensive conductive thermoplastics and a custom-made setup. We used fused filament fabrication (FFF) to manufacture the strain sensors using a dual extruder of conductive and non-conductive commercial materials, following recent work (Stano et al., 2020a, 2020b; Stano et al., 2020a, 2020b; Stano et al., 2022). According to Goh et al. (2022), in order to achieve multi-material printing, the FFF technique can be easily scaled into a multiextruder system, allowing each extruder to squeeze out a different material. The major advantage of using this technique is that it minimizes the impact of structural integrity due to mismatch of material, as the conductive thermoplastic filament can usually bond well with the underlying thermoplastic. Various piezoresistive sensor designs have been successfully fabricated and demonstrated using the FFF technique (Christ et al.; Maurizi et al., 2019; R. Yu et al., 2020). "Summary of 3D printing methods" presented as Table 1 by Jiang et al. (2023) illustrates that extrusion-based 3D printing methods like fused deposition modeling (FDM) is more suited to printing thermoplastics than other techniques like inkjet printing (Lo et al., 2019), liquid resin-based (Shi et al., 2019) and aerosol jet printing (Verma et al., 2022). FDM technique (FFF) has many advantages over polyjet printing according to Xometry (2022). They pointed out that FDM printing materials are cheaper than those for polyJet, faster builds are possible with FDM using low resolution, FDM wastes less material and FDM machines require less maintenance.

The 3D printed conductive thermoplastic polyurethane (CTPU) (namely NinjaTek Eel, NinjaTek, USA, material information provided in Table 5) are embedded in a thin silicone skirt and we performed characterization experiments. The sensors are piezoresistive and change in resistance in response to applied bending or applied load. In addition,

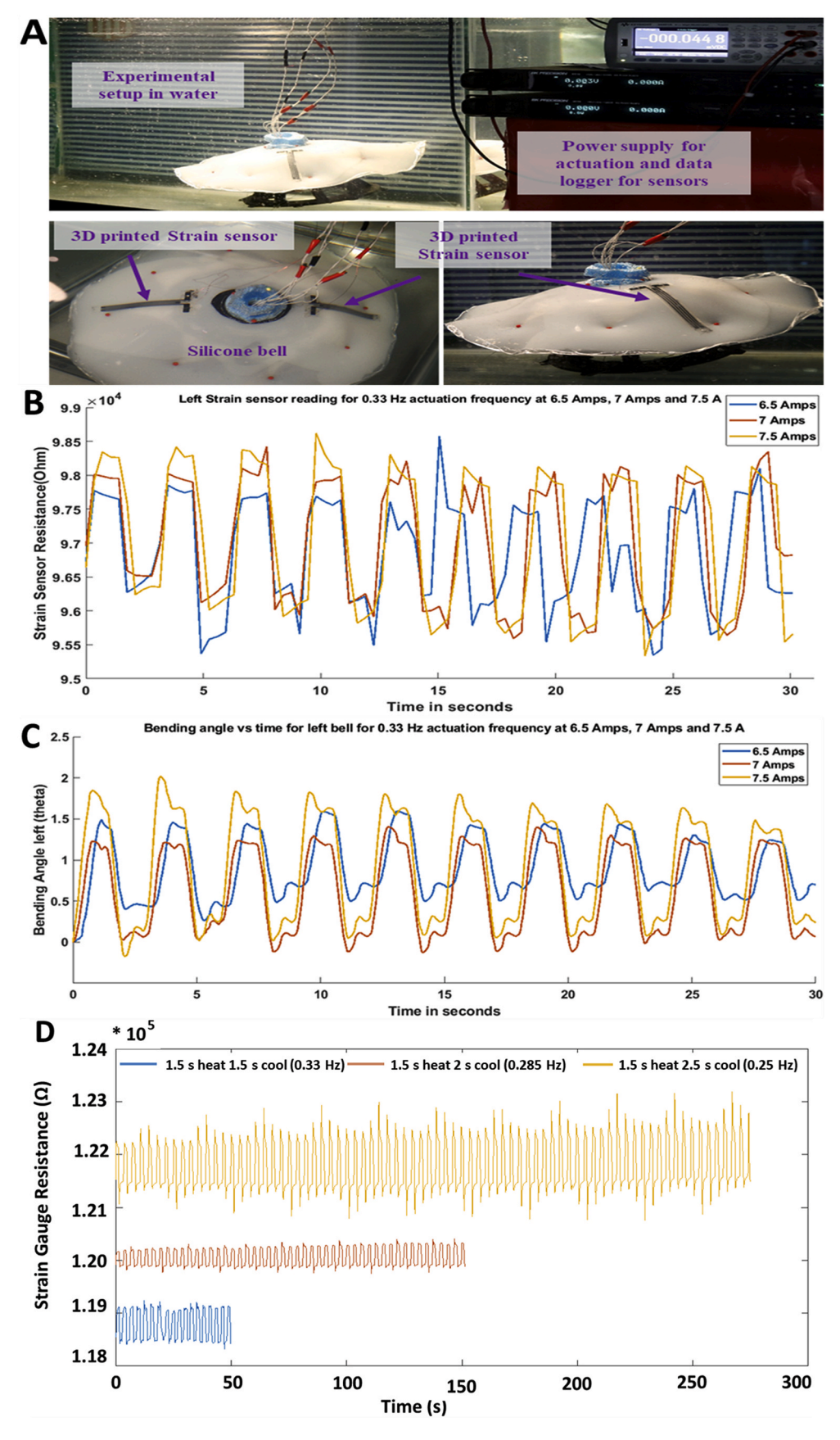


Fig. 8. Flexible strain sensors integrated in the bell segment for estimation of bending angles during actuation. A) Experimental setup for strain sensor for three different actuation frequencies, Top view of jellyfish robot showing the placement of sensors in the bell, (B) Output of the strain 3D printed flexible sensor at 0.33 Hz frequency for three actuation currents, and (C) The bending angle of the bell at 0.33 Hz corresponding to three actuation currents, (D) The change in resistance vs time plot for three different actuation frequencies of the bell (0.33 Hz, 0.285 Hz, and 0.25 Hz), while the robot is swimming.

P. Singh Matharu et al. Ocean Engineering 279 (2023) 114427

the sensors respond to change in temperature and such properties were also determined in a chamber that varies the temperature in a range between -5 °C and 50 °C. A strong link exist between resistance and temperature (Ragolia et al., 2021).

Fig. 8A shows the experimental setup and test results of the strain sensors during different actuation of the bell. Two strain sensors were integrated in the silicone skirt to determine the bending angle, the change in resistance vs time for three different actuation current magnitudes (6.5 A, 76 A and 7.5 A) at 0.33 Hz (Fig. 8B and C) while the jellyfish is actuating. The amplitude of the change in resistance is $1.5\,\mathrm{k}\Omega$ and the bias is $97\,\mathrm{k}\Omega$, which can be clearly seen. The reason for the bias could be the heating of surrounding water in the tank due to the actuation of the SMA coils. It is assumed that as the temperature of water rises the mean resistance offered by the sensor also rises. These sensors respond very fast, they are flexible, and we can easily 3D print them for deploying them for practical applications. We conveniently fabricated 20 to 30 samples using our 3D printing setup. More results can be found in the supplementary file.

Funding

This work was supported by the U.S. Office of Naval Research award "Phase II project: MEDUSAE #N68335-19-C-0303". We would like to thank Dr. Tom McKenna for the financial support and Boston Engineering for the collaboration and discussion.

Data and materials availability

All data needed to evaluate the conclusions in the paper are present in the paper or the Supplementary Materials.

CRediT authorship contribution statement

Pawandeep S. Matharu: Conceptualization, developed the CAD models, vehicle and conducted experiments and theoretical study, Writing – original draft. Zhong Wang: provided the twistron. John H. Costello: studied the real animal characteristics and developed guidelines for linear swimming of jellyfish-inspired robots, guided the research, Writing – review & editing. Sean P. Colin: studied the real animal characteristics and developed guidelines for linear swimming of jellyfish-inspired robots, guided the research, Writing – review & editing. Ray H. Baughman: guided the research, Writing – review & editing. Yonas T. Tadesse: Conceptualization, guided the research, Writing – review & editing.

Declaration of competing interest

The authors declare that they have no known competing financial interests or personal relationships that could have appeared to influence the work reported in this paper.

Data availability

Data will be made available on request.

Acknowledgments

We gratefully acknowledge Ms. Tian Yi for helping in 3D printing different prototypes and Dr. Gianni Stano for 3D printing strain sensors. We would like to thank Dr. Yara Almubarak and Dr. Armita Hamidi for the preliminary experiments in wave energy harvesting using twistron.

Appendix A. Supplementary data

Supplementary data to this article can be found online at https://doi.org/10.1016/j.oceaneng.2023.114427.

References

- Ahlborn, B.K., Blake, R.W., Megill, W.M., 2006. Frequency tuning in animal locomotion. Zoology 109 (1), 43–53.
- Alejandre, A., Olszewski, O.Z., Jackson, N., 2017. Actuation Control of a PiezoMEMS Biomimetic Robotic Jellyfish.
- Almubarak, Y., Punnoose, M., Maly, N.X., Hamidi, A., Tadesse, Y., 2020a. KryptoJelly: a Jellyfish Robot with Confined, Adjustable Pre-stress, and Easily Replaceable Shape Memory Allov NiTi Actuators.
- Almubarak, Y., Punnoose, M., Maly, N.X., Hamidi, A., Tadesse, Y., 2020b. KryptoJelly: a jellyfish robot with confined, adjustable pre-stress, and easily replaceable shape memory alloy NiTi actuators. Smart Mater. Struct. 29 (7), 075011.
- Barbar, A., Joseph, N., Donald, L., John, B., 2011. Design and development of bioinspired underwater jellyfish like robot using ionic polymer metal composite (IPMC) actuators. Paper presented at the Proc.SPIE.
- Biewener, A.A., 2003. Animal Locomotion. Oxford University Press, Oxford [England]; New York, 2003.
- Bu, K., Gong, X., Yu, C., Xie, F., 2022. Biomimetic aquatic robots based on fluid-driven actuators: a review. J. Mar. Sci. Eng. 10 (6), 735.
- Bujard, T., Giorgio-Serchi, F., Weymouth, G.D., 2021. A resonant squid-inspired robot unlocks biological propulsive efficiency. Sci. Robotics 6 (50), eabd2971.
- Cheng, T., Li, G., Liang, Y., Zhang, M., Liu, B., Wong, T.-W., Li, T., 2018a. Untethered soft robotic jellyfish. Smart Mater. Struct. 28 https://doi.org/10.1088/1361-665X/ poed/ff
- Cheng, T., Li, G., Liang, Y., Zhang, M., Liu, B., Wong, T.W., Li, T., 2018b. Untethered soft robotic jellyfish. Smart Mater. Struct. 28 https://doi.org/10.1088/1361-665X/ aaed4f
- Christ, J.F., Hohimer, C.J., Aliheidari, N., Ameli, A., Mo, C., Pötschke, P., 2017/04/1. 3D Printing of Highly Elastic Strain Sensors Using Polyurethane/multiwall Carbon Nanotube Composites.
- Christianson, C., Bayag, C., Li, G., Jadhav, S., Giri, A., Agba, C., Tolley, M.T., 2019. Jellyfish-inspired soft robot driven by fluid electrode dielectric organic robotic actuators. Front. Robotics AI 6. https://doi.org/10.3389/frobt.2019.00126, 126-126.
- Chu, H., Hu, X., Wang, Z., Mu, J., Li, N., Xiaoshuang, Z., Baughman, R., 2021. Unipolar stroke, electroosmotic pump carbon nanotube yarn muscles. Science 371, 494–498. https://doi.org/10.1126/science.abc4538.
- Colin, S.P., Costello, J.H., Dabiri, J.O., Villanueva, A., Blottman, J.B., Gemmell, B.J., Priya, S., 2012. Biomimetic and live medusae reveal the mechanistic advantages of a flexible bell margin. PLoS One 7 (11), e48909.
- Costello, J., Colin, S., Gemmell, B., Dabiri, J., 2019. Hydrodynamics of vortex generation during bell contraction by the hydromedusa eutonina indicans (romanes, 1876). Biomimetics 4. https://doi.org/10.3390/biomimetics4030044, 44-44.
- Costello, J.H., Colin, S.P., Dabiri, J.O., 2008. Medusan morphospace: phylogenetic constraints, biomechanical solutions, and ecological consequences. Invertebr. Biol. 127 (3), 265–290. https://doi.org/10.1111/j.1744-7410.2008.00126.x.
- Costello, J.H., Colin, S.P., Dabiri, J.O., Gemmell, B.J., Lucas, K.N., Sutherland, K.R., 2021. The hydrodynamics of jellyfish swimming. Ann. Rev. Mar. Sci 13 (June), 375–396. https://doi.org/10.1146/annurev-marine-031120-091442.
- Dabiri, J.O., Colin, S.P., Costello, J.H., 2006. Fast-swimming Hydromedusae Exploit Velar Kinematics to Form an Optimal Vortex Wake, pp. 2025–2033. https://doi.org/ 10.1242/jeb.02242.
- Dabiri, J.O., Colin, S.P., Costello, J.H., Gharib, M., 2005. Flow Patterns Generated by Oblate Medusan Jellyfish: Field Measurements and Laboratory Analyses, pp. 1257–1265. https://doi.org/10.1242/jeb.01519, 1997.
- Daniel, L., 1983. Mechanics and Energetics of Medusan Jet Propulsion.
- Daudpoto, J., Memon, A., Hussain, I., 2012. Actuation Characteristics of 0.15 Mm Diameter Flexinol® and Biometal® Wire Actuators for Robotic Applications, 32. Mehran University Research Journal of Engineering & Technology, pp. 147–152.
- Demont, M.E., Gosline, J.M., 1988. Mechanics of jet propulsion in the hydromedusan jellyfish, polyorchis pexicillatus: I. Mechanical properties of the locomotor structure. J. Exp. Biol. 134 (1), 313–332. https://doi.org/10.1242/jeb.134.1.313.
- Dynalloy (2021). (FLEXINOL® Actuator Spring Technical and Design Data]). Elahinia, M., Shayesteh Moghaddam, N., Taheri Andani, M., Amerinatanzi, A., Bimber, B. A., Hamilton, R.F., 2016. Fabrication of NiTi through additive manufacturing: a review. Prog. Mater. Sci. 83, 630–663. https://doi.org/10.1016/j.
- Frame, J., Lopez, N., Curet, O., Engeberg, E.D., 2018a. Thrust force characterization of free-swimming soft robotic jellyfish. Bioinspiration Biomimetics 13 (6), 64001-64001
- Frame, J., Lopez, N., Curet, O., Engeberg, E.D., 2018b. Thrust Force Characterization of Free-Swimming Soft Robotic Jellyfish.
- Furst, S.J., Seelecke, S., 2012. Modeling and experimental characterization of the stress, strain, and resistance of shape memory alloy actuator wires with controlled power input. J. Intell. Mater. Syst. Struct. 23 (11), 1233–1247. https://doi.org/10.1177/ 1045389X12445036.
- Garcia-Cordova, F., González, A., 2013. Intelligent navigation for a solar powered unmanned underwater vehicle. Int. J. Adv. Rob. Syst. 10 https://doi.org/10.5772/ 56020
- Gemmell, B.J., Costello, J.H., Colin, S.P., Stewart, C.J., Dabiri, J.O., Tafti, D., Priya, S., 2013. Passive energy recapture in jellyfish contributes to propulsive advantage over other metazoans. Proc. Natl. Acad. Sci. USA 110 (44), 17904–17909. https://doi. org/10.1073/pnas.1306983110.
- Giorgio-Serchi, F., Lidtke, A.K., Weymouth, G.D., 2018. A soft aquatic actuator for unsteady peak power amplification. IEEE/ASME Transact. Mechatronics 23 (6), 2968–2973. https://doi.org/10.1109/TMECH.2018.2873253.

P. Singh Matharu et al. Ocean Engineering 279 (2023) 114427

- Godaba, H., Li, J., Wang, Y., Zhu, J., 2016. A soft jellyfish robot driven by a dielectric elastomer actuator. IEEE Rob. Autom. Lett. 1 (2), 624–631. https://doi.org/ 10.1109/J.RA.2016.2522498.
- Goh, G.D., Goh, G.L., Lyu, Z., Ariffin, M.Z., Yeong, W.Y., Lum, G.Z., Wong, H.Y.A., 2022.
 3D printing of robotic soft grippers: toward smart actuation and sensing. Advanced Materials Technologies 7 (11), 2101672. https://doi.org/10.1002/admt.202101672.
- Hamidi, A., Almubarak, Y., Rupawat, Y., Warren, J., Tadesse, Y., 2020a. Poly-saora robotic jellyfish: swimming underwater by twisted and coiled polymer actuators. Smart Mater. Struct. 29 https://doi.org/10.1088/1361-665X/ab7738.
- Hamidi, A., Almubarak, Y., Rupawat, Y.M., Warren, J., Tadesse, Y., 2020b. Poly-Saora robotic jellyfish: swimming underwater by twisted and coiled polymer actuators. Smart Mater. Struct. 29 (4), 045039.
- Hamidi, A., Almubarak, Y., Tadesse, Y., 2019. Multidirectional 3D-printed functionally graded modular joint actuated by TCPFL muscles for soft robots. Bio-Design Manufact. 2 (4), 256–268. https://doi.org/10.1007/s42242-019-00055-6.
- Hamidi, A., Tadesse, Y., 2019. 3D printing of very soft elastomer and sacrificial carbohydrate glass/elastomer structures for robotic applications. Mater. Des. 187, 108324 https://doi.org/10.1016/j.matdes.2019.108324.
- Hareesh, G., Li, J., Wang, Y., Zhu, J., 2016. A soft jellyfish robot driven by a dielectric elastomer actuator. IEEE Rob. Autom. Lett. 1 https://doi.org/10.1109/ LRA.2016.2522498, 1-1.
- Hoover, A., Miller, L., 2015. A numerical study of the benefits of driving jellyfish bells at their natural frequency. J. Theor. Biol. 374, 13–25. https://doi.org/10.1016/j. jtbi.2015.03.016.
- Ilievski, F., Mazzeo, A.D., Shepherd, R.F., Chen, X., Whitesides, G.M., 2011. Soft robotics for chemists. Angew. Chem. 123 (8), 1930–1935.
- Jiang, Y., Islam, M.N., He, R., Huang, X., Cao, P.F., Advincula, R.C., Choi, W., 2023. Recent advances in 3D printed sensors: materials, design, and manufacturing. Advanced Materials Technologies 8 (2), 2200492.
- Joshi, A., Kulkarni, A., Tadesse, Y., 2019. FludoJelly: experimental study on jellyfish-like soft robot enabled by soft pneumatic composite (SPC). Robotics 8 (3). https://doi. org/10.3390/robotics8030056.
- Kadiyam, J., Mohan, S., 2019. Conceptual design of a hybrid propulsion underwater robotic vehicle with different propulsion systems for ocean observations. Ocean Eng. 182, 112–125.
- Katzschmann, R.K., DelPreto, J., MacCurdy, R., Rus, D., 2018. Exploration of underwater life with an acoustically controlled soft robotic fish. Sci. Robotics 3 (16).
- Kazemi-lari, M., Dostine, A., Zhang, J., Wineman, A., Shaw, J., 2019. Robotic Jellyfish Actuated with a Shape Memory Alloy Spring.
- Kim, S.H., Haines, C.S., Li, N., Kim, K.J., Mun, T.J., Choi, C., Bykova, J., 2017. Harvesting electrical energy from carbon nanotube yarn twist. Science 357 (6353), 773–778.
- Krieg, M., Mohseni, K., 2008. Thrust characterization of a bioinspired vortex ring thruster for locomotion of underwater robots. IEEE J. Ocean. Eng. 33 (2), 123–132. https://doi.org/10.1109/JOE.2008.920171.
- Lara-Quintanilla, A., Bersee, H.E.N., 2015. Active cooling and strain-ratios to increase the actuation frequency of SMA wires. Shape Memory Superelast. 1 (4), 460–467. https://doi.org/10.1007/s40830-015-0038-8.
- Lee, H.-T., Kim, M.-S., Lee, G.-Y., Kim, C.-S., Ahn, S.-H., 2018. Shape memory alloy (SMA)-Based microscale actuators with 60% deformation rate and 1.6 kHz actuation speed. Small 14. https://doi.org/10.1002/smll.201801023, 1801023-1801023.
- Lepró, X., Ovalle-Robles, R., Lima, M.D., Elías, A.L., Terrones, M., Baughman, R.H., 2012. Catalytic twist-spun yarns of nitrogen-doped carbon nanotubes. Adv. Funct. Mater. 22 (5), 1069–1075.
- Li, G., Chen, X., Zhou, F., Liang, Y., Xiao, Y., Cao, X., Yang, W., 2021. Self-powered soft robot in the mariana trench. Nature 591 (7848), 66–71. https://doi.org/10.1038/ s41586-020-03153-7
- Li, M., Tang, Y., Soon, R. H., Dong, B., Hu, W., & Sitti, M. Miniature coiled artificial muscle for wireless soft medical devices. Sci. Adv., 8(10), eabm5616. doi:10.1126/ sciadv.abm5616.
- Li, T., Li, G., Liang, Y., Cheng, T., Dai, J., Yang, X., Luo, Y., 2017. Fast-moving soft electronic fish. Sci. Adv. 3 (4), e1602045.
- Li, Y., Xu, Y., Wu, Z., Ma, L., Guo, M., Li, Z., Li, Y., 2022. A comprehensive review on fish-inspired robots. Int. J. Adv. Rob. Syst. 19 (3), 17298806221103707.
- Lianjun, W., Monica Jung de, A., Richard, S.R., Carter, H., Marcio, D.L., Ray, H.B., Yonas, T., 2015. Nylon-muscle-actuated robotic finger. Paper presented at the Proc. SPIE
- Lo, L.-W., Shi, H., Wan, H., Xu, Z., Tan, X., Wang, C., 2019. Inkjet-printed soft resistive pressure sensor patch for wearable electronics applications. Advanced Materials Technologies 5, 1900717. https://doi.org/10.1002/admt.201900717.
- Marut, K., Stewart, C., Michael, T., Villanueva, A., Priya, S., 2013. A jellyfish-inspired jet propulsion robot actuated by an iris mechanism. Smart Mater. Struct. 22 (9), 094021 https://doi.org/10.1088/0964-1726/22/9/094021.
- Matharu, P.S., Ghadge, A.A., Almubarak, Y., Tadesse, Y., 2022. Jelly-Z: twisted and coiled polymer muscle actuated jellyfish robot for environmental monitoring. ACTA IMEKO 11 (3), 1–7.
- Maurizi, M., Slavič, J., Cianetti, F., Jerman, M., Valentinčič, J., Lebar, A., Boltežar, M., 2019. Dynamic measurements using FDM 3D-printed embedded strain sensors. Sensors 19 (12). https://doi.org/10.3390/s19122661. Retrieved from.
- Megill, W.M., Gosline, J.M., Blake, R.W., 2005. The modulus of elasticity of fibrillincontaining elastic fibres in the mesoglea of the hydromedusa Polyorchis penicillatus. J. Exp. Biol. 208 (Pt 20), 3819–3834. https://doi.org/10.1242/jeb.01765.
- Michael, T., Tolley, R.F.S., Bobak Mosadegh, Kevin, Galloway, C., Wehner, Michael, Karpelson, Michael, Wood, Robert J., Whitesides, George M., 2014. A resilient, untethered soft robot. Soft Robot. https://doi.org/10.1089/soro.2014.0008.
- Miles, J.G., Battista, N.A., 2019. Don't be jelly. Exploring Effect. Jellyfish Locomotion. arXiv preprint arXiv:1904.09340.

Mu, J., Jung de Andrade, M., Fang, S., Wang, X., Gao, E., Li, N., Baughman, R.H., 2019. Sheath-run artificial muscles. Science 365, 150–155.

- Nagata, R.M., Morandini, A.C., Colin, S.P., Migotto, A.E., Costello, J.H., 2016. Transitions in morphologies, fluid regimes, and feeding mechanisms during development of the medusa Lychnorhiza lucerna. Mar. Ecol. Prog. Ser. 557, 145–159.
- Najem, J., Sarles, A., Akle, B., Leo, D., 2012. Biomimetic jellyfish-inspired underwater vehicle actuated by ionic polymer metal composite actuators. Smart Mater. Struct.-SMART MATER STRUCT. 21 https://doi.org/10.1088/0964-1726/21/9/094026.
- Nawroth, J.C., Lee, H., Feinberg, A.W., Ripplinger, C.M., McCain, M.L., Grosberg, A., Parker, K.K., 2012. Letters A tissue-engineered jellyfish with biomimetic propulsion. Nat. Biotechnol. 30 (8), 792–797. https://doi.org/10.1038/nbt.2269.
- Ninjatek, 2023. EEL 3D PRINTER FILAMENT (90A). Retrieved from. https://ninjatek.com/shop/eel/.
- Nizamani, A.M., Daudpoto, J., Nizaman, M.A., 2017. Development of Faster SMA Actuators. Shape Memory Alloys - Fundamentals And Applications. https://doi.org/ 10.5772/intechopen.69868.
- Paley, D.A., Wereley, N.M., 2020. Bioinspired Sensing, Actuation, and Control in Underwater Soft Robotic Systems. Springer International Publishing AG, Cham.
- Paraz, F., Schouveiler, L., Eloy, C., 2016. Thrust generation by a heaving flexible foil: resonance, nonlinearities, and optimality. Phys. Fluids 28, 011903. https://doi.org/ 10.1063/1.4939449.
- Park, S.-J., Gazzola, M., Park, K.S., Park, S., Di Santo, V., Blevins, E.L., Parker, K.K., 2016. Phototactic guidance of a tissue-engineered soft-robotic ray. Science 353 (6295), 158–162. https://doi.org/10.1126/science.aaf4292.
- Park, Y.-L., Chen, B.-r., Pérez-Arancibia, N.O., Young, D., Stirling, L., Wood, R.J., Nagpal, R., 2014. Design and control of a bio-inspired soft wearable robotic device for ankle–foot rehabilitation. Bioinspiration Biomimetics 9 (1), 016007. https://doi. org/10.1088/1748-3182/9/1/016007.
- Park, Y.-L., Majidi, C., Kramer, R., Bérard, P., Wood, R.J., 2010. Hyperelastic pressure sensing with a liquid-embedded elastomer. J. Micromech. Microeng. 20 (12), 125029
- Piao, C., Suk, J.W., 2020. Graphene/silver nanoflower hybrid coating for improved cycle performance of thermally-operated soft actuators. Sci. Rep. 10 (1), 17553 https:// doi.org/10.1038/s41598-020-74641-5.
- Picardi, G., Chellapurath, M., Iacoponi, S., Stefanni, S., Laschi, C., Calisti, M., 2020. Bioinspired underwater legged robot for seabed exploration with low environmental disturbance. Sci. Robotics 5 (42), 1–15. https://doi.org/10.1126/SCIROBOTICS. AAZ1012.
- Polygerinos, P., Wang, Z., Galloway, K.C., Wood, R.J., Walsh, C.J., 2015. Soft robotic glove for combined assistance and at-home rehabilitation. Robot. Autonom. Syst. 73, 135–143. https://doi.org/10.1016/j.robot.2014.08.014.
- Pugi, L., Allotta, B., Pagliai, M., 2018. Redundant and reconfigurable propulsion systems to improve motion capability of underwater vehicles. Ocean Eng. 148, 376–385.
- Ragolia, M.A., Di Nisio, A., Lanzolla, A.M., Percoco, G., Scarpetta, M., Stano, G., 2021. Thermal characterization of electrical resistance of 3D printed sensors. In: Paper Presented at the 2021 IEEE International Instrumentation and Measurement Technology Conference (IZMTC).
- Raj, A., Thakur, A., 2016. Fish-inspired robots: design, sensing, actuation, and autonomy—a review of research. Bioinspiration Biomimetics 11, 031001. https://doi.org/10.1088/1748-3190/11/3/031001.
- Ramananarivo, S., Godoy-Diana, R., Thiria, B., 2011. Rather than resonance, flapping wing flyers may play on aerodynamics to improve performance. Proc. Natl. Acad. Sci. U. S. A 108, 5964–5969. https://doi.org/10.1073/pnas.1017910108.
- Ren, Z., Hu, W., Dong, X., Sitti, M., 2019a. Multi-functional soft-bodied jellyfish-like swimming. Nat. Commun. 10 (1) https://doi.org/10.1038/s41467-019-10549-7.
- Ren, Z., Wang, T., Hu, W., Sitti, M., 2019b. A Magnetically-Actuated Untethered Jellyfish-Inspired Soft Milliswimmer.
- Ruiz, L.A., Whittlesey, R.W., Dabiri, J.O., 2011. Vortex-enhanced propulsion. J. Fluid Mech. 668, 5–32. https://doi.org/10.1017/S0022112010004908.
- Rumson, A.G., 2021. The application of fully unmanned robotic systems for inspection of subsea pipelines. Ocean Eng. 235, 109214.
- Sachyani Keneth, E., Kamyshny, A., Totaro, M., Beccai, L., Magdassi, S., 2021. 3D printing materials for soft robotics. Adv. Mater. 33 (19), 2003387 https://doi.org/10.1002/adma.202003387.
- Scaradozzi, D., Palmieri, G., Costa, D., Pinelli, A., 2017. BCF swimming locomotion for autonomous underwater robots: a review and a novel solution to improve control and efficiency. Ocean Eng. 130, 437–453.
- Shi, H., Al-Rubaiai, M., Holbrook, C., Miao, J., Pinto, T., Wang, C., Tan, X., 2019. Screen-printed soft capacitive sensors for spatial mapping of both positive and negative pressures. Adv. Funct. Mater. 29, 1809116 https://doi.org/10.1002/adfm.201809116.
- Sivčev, S., Coleman, J., Omerdić, E., Dooly, G., Toal, D., 2018. Underwater manipulators: a review. Ocean Eng. 163, 431–450.
- Siemiński, Przemysław, 2021. Introduction to fused deposition modeling. InAdditive Manufact. 217–275. Elsevier.
- Smooth-On.com, 2022. EcoflexTM 00-10. Retrieved from. https://www.smooth-on.com/products/ecoflex-00-10/?pk_campaign=dynamicsearch&pk_kwd=&gclid=Cjw_KCAiA55mPBhBOEiwANmzoQoAH5TR6PvE9yfiDaQ8BTez1hHFuMffDWn_iAI36IzX2c5z9XUDjoyBoCAG8QAvD_BwE.
- Stano, G., Di Nisio, A., Lanzolla, A., Percoco, G., 2020a. Additive manufacturing and characterization of a load cell with embedded strain gauges. Precis. Eng. 62, 113–120.
- Stano, G., Di Nisio, A., Lanzolla, A.M., Ragolia, M., Percoco, G., 2020b. Fused filament fabrication of commercial conductive filaments: experimental study on the process

- parameters aimed at the minimization, repeatability and thermal characterization of electrical resistance. Int. J. Adv. Des. Manuf. Technol. 111 (9), 2971–2986.
- Stano, G., Ovy, S.M.A.I., Edwards, J., Cianchetti, M., Percoco, G., Tadesse, Y., 2022. One-shot additive manufacturing of robotic finger with embedded sensing and actuation. Int. J. Adv. Des. Manuf. Technol. 124, 1–19. https://doi.org/10.1007/s00170-022-10556-x
- Stratasys, 2023. FDM TPU 92A product data sheet. Retrieved from. https://www.stratasys.com/siteassets/materials/materials-catalog/fdm-materials/tpu-92a/fdm-tpu-92a-3d-printing-material-data-sheet a.pdf?v=48e22c.
- Suzumori, K., likura, S., Tanaka, H., 1992. Applying a flexible microactuator to robotic mechanisms. IEEE Control Syst. Mag. 12 (1), 21–27. https://doi.org/10.1109/ 37.120448
- Tadesse, Y., Thayer, N., Priya, S., 2010. Tailoring the response time of shape memory alloy wires through active cooling and pre-stress. J. Intell. Mater. Syst. Struct. 21, 19–40. https://doi.org/10.1177/1045389X09352814.
- Tadesse, Y., Villanueva, A., Haines, C., Novitski, D., Baughman, R., Priya, S., 2012. Hydrogen-fuel-powered bell segments of biomimetic jellyfish. Smart Mater. Struct. 21 (4), 45013-45013.
- Tang, W., Lin, Y., Zhang, C., Liang, Y., Wang, J., Wang, W., . . . Zou, J. Self-contained soft electrofluidic actuators. Sci. Adv., 7(34), eabf8080. doi:10.1126/sciadv.abf8080.
- Uchino, K., 2018. Piezoelectric energy harvesting systems—essentials to successful developments. Energy Technol. 6 (5), 829–848. https://doi.org/10.1002/ epte.2017.00785
- Verma, A., Goos, R., Weerdt, J.D., Pelgrims, P., Ferraris, E., 2022. Design, fabrication, and testing of a fully 3D-printed pressure sensor using a hybrid printing approach. Sensors 22 (19). https://doi.org/10.3390/s22197531. Retrieved from.
- Villanueva, A., Bresser, S., Chung, S., Tadesse, Y., Priya, S., 2009a. Jellyfish Inspired Unmanned Underwater Vehicle (a) (b), 7287, pp. 1–12. https://doi.org/10.1117/ 12.815754
- Villanueva, A., Bresser, S., Chung, S., Tadesse, Y., Priya, S.J., 2009b. Jellyfish Inspired Underwater Unmanned Vehicle, 7287.
- Villanueva, A., Smith, C., Priya, S., 2011. A biomimetic robotic jellyfish (Robojelly) actuated by shape memory alloy composite actuators. Bioinspiration Biomimetics 6 (3), 036004. https://doi.org/10.1088/1748-3182/6/3/036004.
- Wallin, T.J., Pikul, J., Shepherd, R.F., 2018. 3D printing of soft robotic systems. Nat. Rev. Mater. 3 (6). 84–100. https://doi.org/10.1038/s41578-018-0002-2.
- Wang, S., Chen, Z., 2021. Modeling of jellyfish inspired robot enabled by dielectric elastomer. Int. J. Intell. Robotics Appl., 0123456789 https://doi.org/10.1007/
- Wang, Z., Mun, T.J., Machado, F., Moon, J., Zhang, M., Aliev, A., Baughman, R., 2022a.
 More powerful twistron carbon nanotube yarn mechanical energy harvesters. Adv.
 Mater. 34 https://doi.org/10.1002/adma.202201826.
- Wang, Z., Mun, T.J., Machado, F.M., Moon, J.H., Fang, S., Aliev, A.E., Hyeon, J.S., 2022b. More powerful twistron carbon nanotube yarn mechanical energy harvesters. Adv. Mater.. 2201826
- Wehner, M., Truby, R.L., Fitzgerald, D.J., Mosadegh, B., Whitesides, G.M., Lewis, J.A., Wood, R.J., 2016. An integrated design and fabrication strategy for entirely soft,

- autonomous robots. Nature 536 (7617), 451–455. https://doi.org/10.1038/nature19100.
- Wu, L., Chauhan, I., Tadesse, Y., 2018. A novel soft actuator for the musculoskeletal system. Adv. Mater. Technol. 3 (5), 1700359.
- Wu, Y., Dong, X., Kim, J.-k., Wang, C., Sitti, M., 2022. Wireless soft millirobots for climbing three-dimensional surfaces in confined spaces. Sci. Adv. 8 (21), eabn3431.
- Xiao, J., Duan, J., Yu, J., 2013a. Design and Implementation of a Novel Biomimetic Robotic Jellyfish.
- Xiao, J., Duan, J., Yu, J., 2013b. Design and implementation of a novel biomimetic robotic jellyfish, 12-14 Dec. 2013. In: Paper Presented at the 2013 IEEE International Conference on Robotics and Biomimetics (ROBIO).
- Xometry, T., 2022. FDM vs. PolyJet: Differences and Comparison. Retrieved from. http s://www.xometry.com/resources/3d-printing/fdm-vs-polyjet-3d-printing/.
- Xu, N., Townsend, J., Costello, J., Colin, S., Gemmell, B., Dabiri, J., 2020. Field testing of biohybrid robotic jellyfish to demonstrate enhanced swimming speeds. Biomimetics 5. https://doi.org/10.3390/biomimetics5040064.
- Xu, N.W., Dabiri, J.O., 2020a. Low-power microelectronics embedded in live jellyfish enhance propulsion. Sci. Adv. 6 (5) https://doi.org/10.1126/sciadv.aaz3194 eaaz3194-eaaz3194.
- Xu, N.W., Dabiri, J.O., 2020b. Low-power Microelectronics Embedded in Live Jellyfish Enhance Propulsion. March), pp. 1–11.
- Yang, X., Chang, L., Pérez-Arancibia, N.O., 2020. An 88-milligram insect-scale autonomous crawling robot driven by a catalytic artificial muscle. Sci. Robotics 5 (45), eaba0015. https://doi.org/10.1126/scirobotics.aba0015.
- Ye, J., Yao, Y.-C., Gao, J.-Y., Chen, S., Zhang, P., Sheng, L., Liu, J., 2022. LM-jelly: liquid metal enabled biomimetic robotic jellyfish. Soft Robot.
- Yin, C., Wei, F., Fu, S., Zhai, Z., Ge, Z., Yao, L., Liu, M., 2021a. Visible light-driven jelly fi sh-like miniature. Swim. Soft Robot. https://doi.org/10.1021/acsami.1c13975.
- Yin, C., Wei, F., Fu, S., Zhai, Z., Ge, Z., Yao, L., Liu, M., 2021b. Visible light-driven jellyfish-like miniature swimming soft robot. ACS Appl. Mater. Interfaces 13 (39), 47147–47154. https://doi.org/10.1021/acsami.1c13975.
- Yoerger, D., Govindarajan, A., Howland, J., Llopiz, J., Wiebe, P., Curran, M., Rock, S., 2021. A hybrid underwater robot for multidisciplinary investigation of the ocean twilight zone. Sci. Robotics 6, eabe1901. https://doi.org/10.1126/scirobotics. abs/1901
- Yu, J., Xiao, J., Li, X., Wang, W., 2016. Towards a Miniature Self-Propelled Jellyfish-like Swimming Robot. October), pp. 1–9. https://doi.org/10.1177/1729881416666796.
- Yu, R., Xia, T., Wu, B., Yuan, J., Ma, L., Cheng, G.J., Liu, F., 2020. Highly sensitive flexible piezoresistive sensor with 3D conductive network. ACS Appl. Mater. Interfaces 12 (31), 35291–35299. https://doi.org/10.1021/acsami.0c09552.
- Zhang, J., Zhang, T., Dong, E., Zhang, C., Lin, Z., Song, Z., Zhang, Y., 2022. Bioinspired hydrogel jellyfish with mechanical flexibility and acoustic transparency. Cell Rep. Phys. Sci. 101081 https://doi.org/10.1016/j.xcrp.2022.101081.
- Zhang, M., Fang, S., Zakhidov, A.A., Lee, S.B., Aliev, A.E., Williams, C.D., Baughman, R. H., 2005. Strong, transparent, multifunctional, carbon nanotube sheets. Science 309 (5738), 1215–1219.
- Zhou, Y., Jin, H., Liu, C., Dong, E., Xu, M., Yang, J., 2016. A Novel Biomimetic Jellyfish Robot Based on a Soft and Smart Modular Structure (SMS).